Electronic Thesis and Dissertation Repository

11-21-2017 11:00 AM

Exploiting Fission Yeast Genetic Interaction Data to Identify Disease-Specific Drug Targets for Tuberous Sclerosis Complex

Ashyad Rayhan
The University of Western Ontario

Supervisor
Dr. Jim Karagiannis
The University of Western Ontario

Graduate Program in Biology
A thesis submitted in partial fulfillment of the requirements for the degree in Master of Science
© Ashyad Rayhan 2017

ABSTRACT

Tuberous sclerosis complex (TSC) is an inherited genetic disorder caused by loss-of-function mutations in either *TSC1* or *TSC2*. Their respective gene products regulate the mechanistic target of rapamycin (mTOR) signaling pathway, which serves as an activator of cellular proliferation, metabolism, and cell survival. Orthologs of the *TSC1* and *TSC2* genes exist in a wide range of organisms, including the commonly used and genetically tractable model eukaryote, *Schizosaccharomyces pombe*. To better understand the functional roles of *S. pombe tsc1* and *tsc2*, I exploited recent advances in genetic interaction biology to identify and characterize genes that modulate the phenotypic effects of *tsc1* and *tsc2* gene deletions. As part of this work, I found *ypa1* (encoding a peptidyl-prolyl cis-trans isomerase) and *fft3* (encoding an ATP-dependent DNA helicase) to be negatively interacting with both *tsc1* and *tsc2*. Importantly, while the loss of either *ypa1* or *fft3* in isolation had negligible effects on colony growth, their loss in *tsc1Δ* or *tsc2Δ* backgrounds resulted in significant growth impediments. Thus, the inhibition of either *ypa1* or *fft3* might represent an "Achilles' heel" of cells defective in *tsc1* or *tsc2* function. Lastly, I found that the negative interaction between *ypa1* and *tsc2* is conserved in mammalian cells. This suggests that the targeted inhibition of the orthologous gene product in humans epitomizes a novel therapeutic strategy to combat the TSC pathology.

Keywords: tuberous sclerosis complex, fission yeast, gene buffering, genetic interaction, synthetic growth defect, mTOR pathway

CO-AUTHORSHIP STATEMENT

This thesis incorporates material that is the result of joint research between Ashyad Rayhan and Adam Faller (under the supervision of Dr. Jim Karagiannis) and between Ashyad Rayhan and Dr. Alexander Timoshenko. A. Faller's contribution is limited to the construction of the *tsc2-R1296P* mutant fission yeast strain and the *tsc2-R1296P ypa1Δ* and *tsc2-R1296P fft3Δ* double mutant strains used in this study. Dr. Timoshenko provided expert guidance with respect to the culturing of mouse embryonic fibroblasts. In all other instances, the experimental work, data analysis, interpretation, and writing were performed by Ashyad Rayhan.

ACKNOWLEDGEMENTS

TABLE OF CONTENTS

LIST OF TABLES

LIST OF FIGURES

LIST OF ABBREVIATIONS

4E-BP1	4E binding protein-1
Akt	Akt serine/threonine kinase
cDNA	complementary DNA
DMEM	Dulbecco's modified eagle's medium
DNA-PK	DNA-dependent protein kinase
DPBS	Dulbecco's phosphate-buffered saline
DSB	double stranded breaks
EMM	Edinburgh minimal medium
FBS	fetal bovine serum
Fft3p	fission yeast gene product of *fft3*
GAP	GTPase activating protein
gDNA	genomic DNA
gRNA	guide RNA
HR	homologous recombination
IR	insulin receptors
LAM	lymphangioleiomyomatosis
MEF	mouse embryonic fibroblasts
mTOR	mechanistic target of rapamycin
mTORC1	mTOR complex 1
mTORC2	mTOR complex 2
NGE	neighboring gene effects

NHEJ	non-homologous end joining
NPD	non-parental ditype
ORF	open reading frame
PCR	polymerase chain reaction
PDK1	phosphoinositide dependent protein kinase-1
Pen-strep	penicillin-streptomycin solution
PI3K	phosphoinositide 3-kinase
PP2A	serine/threonine protein phosphatase 2A
PTPA	phosphotyrosyl phosphatase activator
Rheb	ras homolog enriched in brain
RNAPII	RNA polymerase II
ROS	reactive oxygen species
S6K1	ribosomal s6 kinase-1
SGA	synthetic genetic array
shRNA	short hairpin RNAs
siRNA	small interfering RNAs
SPA	sporulation agar
TAE	tris-acetic EDTA
Tor	fission yeast target of rapamycin
TrypLE	cell culture dissociation agent
TSC	tuberous sclerosis complex
tsc1	fission yeast gene encoding hamartin
TSC1	human gene encoding hamartin

Tsc1p   fission yeast hamartin

tsc2   fission yeast gene encoding tuberin

TSC2   human gene encoding tuberin

Tsc2p   fission yeast tuberin

YES   yeast extract with supplements

Ypa1p   fission yeast gene product of *ypa1*

CHAPTER I: INTRODUCTION

1.1 Tuberous sclerosis complex

Tuberous sclerosis complex (TSC) is an autosomal dominant genetic disorder with an occurrence of approximately 1 in 8,000 live births (Rosner et al., 2004; Rosser et al., 2006). The disease causes benign tumors (known as hamartomas) in the brain, heart, kidneys, lungs, and eyes (Napolioni and Curatolo, 2008; Roux et al., 2004). Moreover, patients often suffer from a variety of skin conditions (e.g. hypomelanotic macules, facial angiofibromas, and forehead plaques) (Rosner et al., 2008). Neurological conditions such as autism, seizures, and learning disabilities are also common among affected individuals (Sampson, 2009; Young and Povey, 1998). Figure 1-1 outlines the major clinical manifestations of the TSC pathology.

Loss of heterozygosity in either *TSC1* gene or the *TSC2* gene is frequently associated with the TSC pathology in humans (Hengstschläger et al., 2001; Jones et al., 1999). The *TSC1* gene on chromosome 9q34 encodes hamartin, a 130-kDa hydrophilic protein containing a transmembrane domain and a coiled-coil domain that mediates protein-protein interactions (van Slegtenhorst et al., 1997; Jozwiak, 2006). The *TSC2* gene on chromosome 16p13.3 encodes tuberin (The European Chromosome 16 Tuberous Sclerosis Consortium, 1993). Tuberin, a protein of approximately 200 kDa, forms an intracellular heterodimeric complex with hamartin to regulate downstream signaling (Jozwiak, 2006; Rosner et al., 2004). This process is regulated by tuberin phosphorylation which prevents both the degradation of tuberin by ubiquitination and the formation of homomeric hamartin complexes (Laplante and Sabatini, 2006; Rosner et al., 2004).
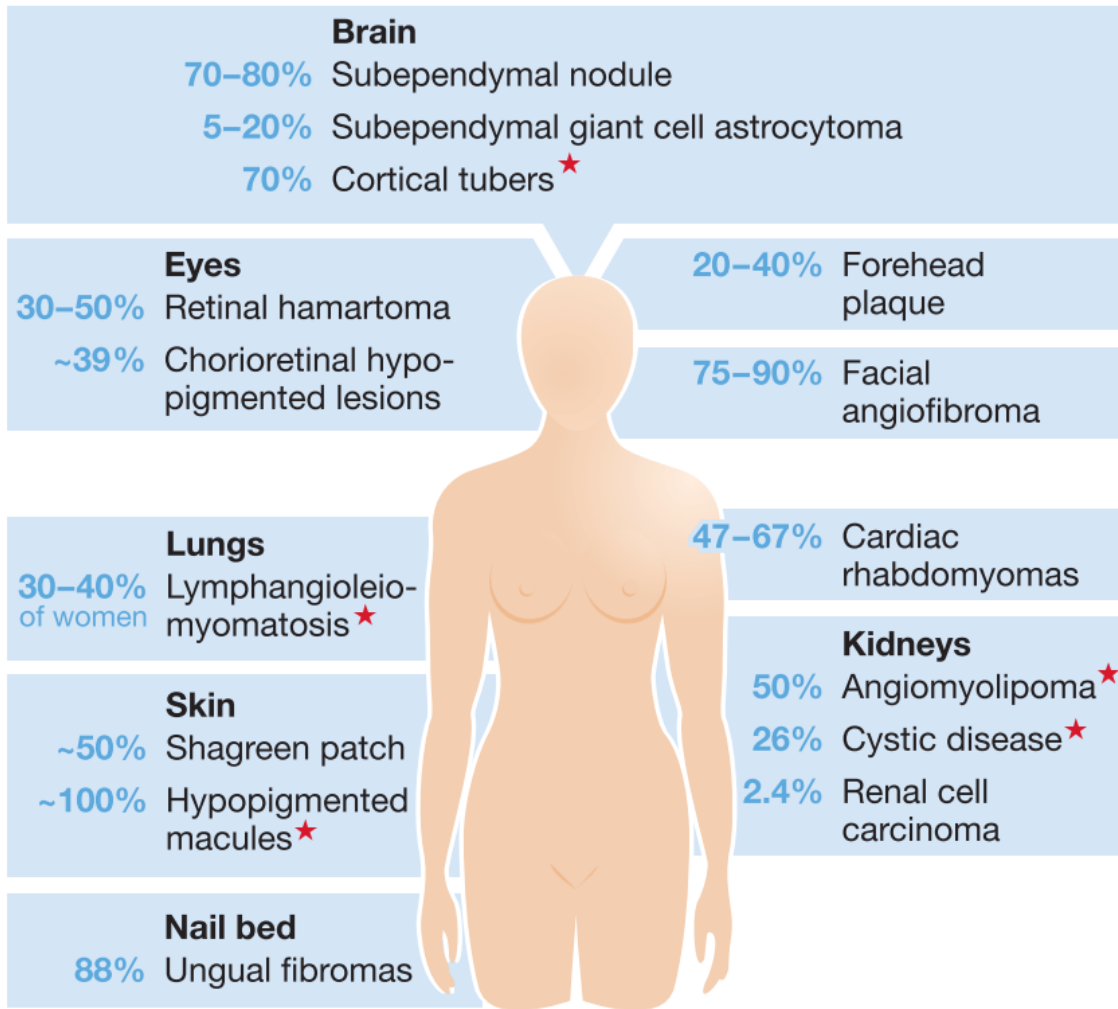
Figure 1-1: The multisystem pathogenesis of tuberous sclerosis complex. A range of tissues and organs are affected in those with TSC. Respective clinical conditions are noted in the blue boxes with percentages representing the corresponding occurrence in patients. Red stars (*) indicate clinical conditions that may arise from alternate TSC-Rheb signaling networks. Reproduced from Neuman and Henske (2011) under the fair use provision of the Canadian Copyright Modernization Act (2012).

The hamartin-tuberin heterodimer is a key upstream component of the mechanistic target of rapamycin (mTOR) signaling pathway (Laplante and Sabatini, 2006). Importantly, homologs of the human TSC1 and TSC2 proteins are found across a range species, demonstrating that the signaling network is highly conserved (Figure 1-2) (Serfontein et al., 2011). Studies have also shown that the TSC1-TSC2 heterodimer act as a tumor suppressing complex to regulate cellular growth and proliferation (Mak and Yeung, 2004; Piedimonte et al., 2006; Roux et al., 2004). Interestingly, TSC-specific tumor progression follows the Knudson two-hit model of oncogenesis (i.e. where an inherited loss of function mutation in one allele and a sporadic loss of function mutation in the remaining allele lead to loss of heterozygosity at either the *TSC1* or *TSC2* locus) (Jozwiak et al., 2008; Mak and Yeung, 2004).

1.2 The Akt-TSC1/2-mTOR signaling pathway

The mTOR signaling pathway plays an important role in regulating cellular growth, proliferation, survival and metabolism (Franz and Weiss, 2012). mTOR is a serine/threonine kinase that belongs to the phosphoinositide 3-kinase (PI3K) related kinase family (Xu et al., 2014). mTOR is evolutionarily conserved and forms the catalytic core of two distinct multi-protein complexes, mTOR complex 1 (mTORC1), and mTOR complex 2 (mTORC2) (Laplante and Sabatini, 2012); together, they promote cell growth in response to positive inputs such as nutrients and growth factors (Menon et al., 2014).

The hamartin-tuberin heterodimer (TSC1-TSC2 complex) is a key upstream regulator of mTORC1 (Laplante and Sabatini, 2012). Tuberin possesses a catalytic GTPase activating protein (GAP) domain and works to negatively regulate the downstream Rheb
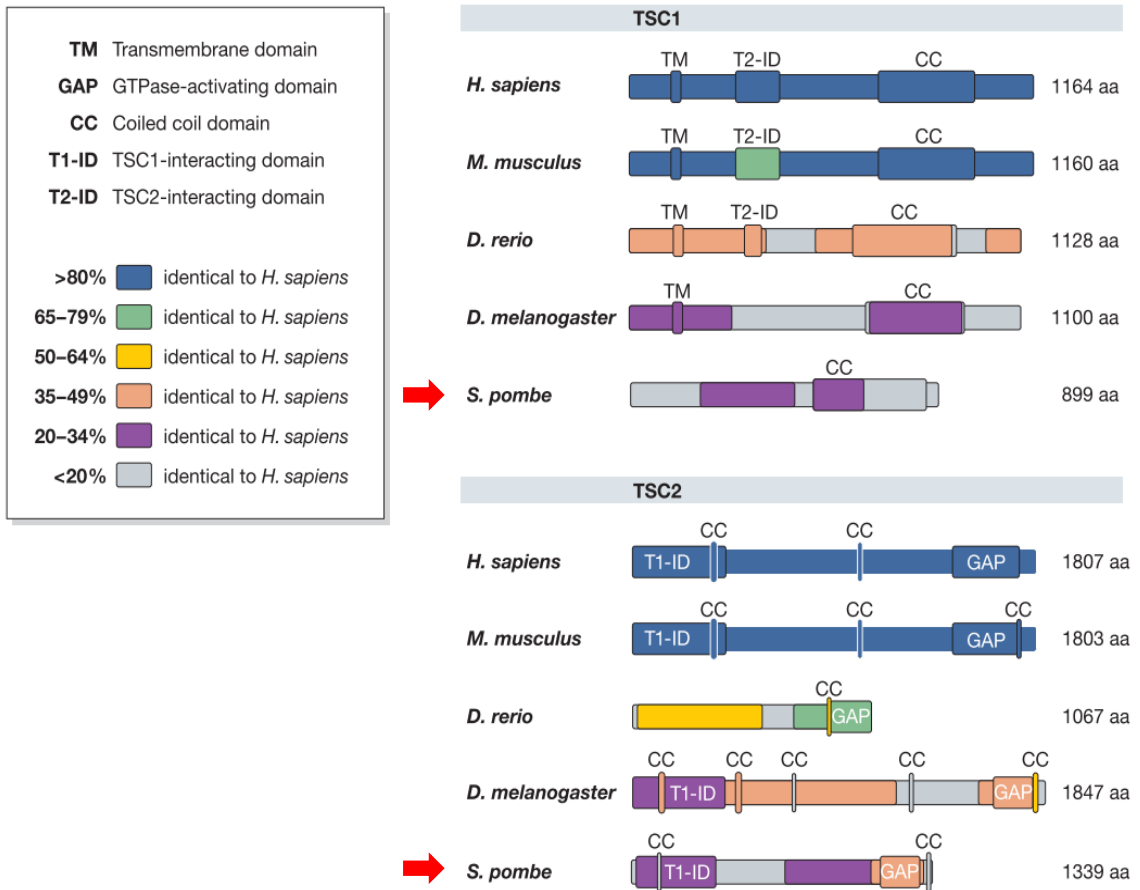
Figure 1-2: The conservation of hamartin and tuberin across species. Domain structure of the TSC1 (hamartin) and TSC2 (tuberin) proteins across species. Various colours indicate the relative level of homology to the orthologous human TSC proteins. The fission yeast Tsc1p and Tsc2p proteins are indicated with a red arrow. The coiled-coil (CC) domains of the human TSC1 and TSC2, in addition to the TSC1 interaction domain (T1-ID) and GAP domain of TSC2 are conserved in *S. pombe*. The TSC2 interaction domain on TSC1 (T2-ID) is not shown to be conserved, but this conclusion is not consistent between different alignments (Serfontein et al., 2011) and studies have shown Tsc1p-Tsc2p heterodimers exist in fission yeast (discussed later). Figure modified from Neuman and Henske (2011) under the fair use provision of the Canadian Copyright Modernization Act (2012).

4

protein (Manning and Cantley, 2003). Rheb (Ras homolog enriched in brain) is rendered inactive (GDP bound) by the negative GTPase activity of tuberin (Laplante and Sabatini, 2012). Once growth factors and nutrients activate the insulin receptors (IR), PI3K can recruit phosphoinositide dependent protein kinase-1 (PDK1) which mediates serine phosphorylation of serine/threonine kinase Akt (Xu et al., 2014). Upon activation, Akt can phosphorylate and subsequently inhibit the TSC1-TSC2 complex; this results in the activation of Rheb (now GTP bound), which mediates the downstream activation of mTORC1 (Astrinidis and Henske, 2005; Benjamin and Hall, 2014; Dalle Pezze et al., 2012). Aforementioned cell growth and proliferation is achieved upon further phosphorylation of several downstream effectors by mTORC1, leading to activation of the ribosomal s6 kinase-1 (p70S6K1) and inhibition of the 4E binding protein-1 (4E-BP1) (Manning and Cantley, 2003).

Adding to the complexity of the Akt-TSC1/2-mTORC1 pathway is a negative feedback loop, initiated by p70S6K1-dependent phosphorylation and inhibition of IRs (Dalle Pezze et al., 2012). Furthermore, low energy levels, hypoxia, and cellular stress are also able to inactivate mTORC1 signaling (Benjamin and Hall, 2014). Growth factors can also modulate mTORC2 activation, however, the complex is geared towards cell survival, metabolism, and cytoskeletal organization (Dalle Pezze et al., 2012; Laplante and Sabatini, 2012). Previous works suggest that mTORC2 activity is dependent on PI3K and is resistant to both rapamycin and the negative feedback loop that moderates mTORC1 activity (Dalle Pezze et al., 2012). Interestingly, mTORC2 activity is independent of Akt-TSC1/2 regulation, suggesting a different regulatory mechanism for this signaling cascade (Dalle Pezze et al., 2012). Figure 1-3 provides a summary of the mTORC1 signaling pathway.
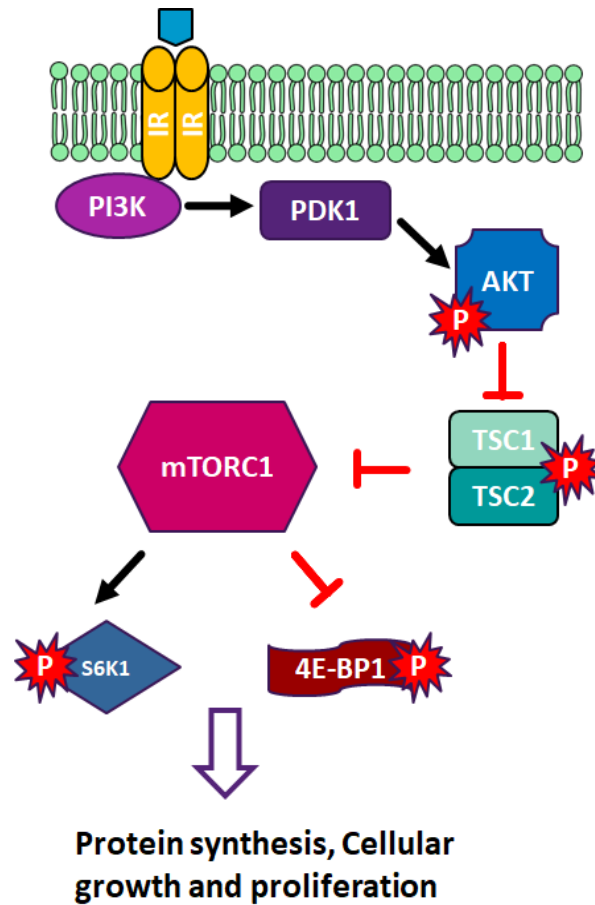
Figure 1-3: The Akt-TSC1/2-mTORC1 signaling cascade. Upon stimulation of the insulin receptors (IRs), the mTORC1 complex promotes increased levels of protein synthesis, inhibition of autophagy, cell growth and proliferation. Upstream kinases – PI3K and PDK1 modulate the phosphorylation and subsequent activation of Akt. Next, pAkt inactivate the TSC1-TSC2 heterodimeric complex, leading to an activated mTORC1. Activated mTORC1 phosphorylates and inhibits downstream 4E-BP1, which would otherwise repress protein translation. In contrast, mTORC1-mediated phosphorylation of S6K1 promotes ribosomal protein synthesis. The pathway is also regulated by several feedback mechanisms (not shown).

1.3 Fission yeast as a model system to study the TSC pathology

The fission yeast *Schizosaccharomyces pombe* is a unicellular organism commonly used in the field of eukaryotic cellular and molecular biology. It is genetically tractable and is often used to examine fundamental cellular processes such as transcription, translation, cell-cycle control, DNA damage and repair, signaling pathways, and epigenetics (Forsburg, 2005; Hoffman et al., 2015).

The *S. pombe* genome has been fully sequenced to reveal ~ 5000 protein-coding genes (ORFs) distributed among three chromosomes (Wood et al., 2002). Among the proteins encoded by the *S. pombe* genome, a subset of 172 proteins share close homology with human disease proteins (Wood et al., 2002). Moreover, the *S. pombe* laboratory strains can be diploid or haploid – carrying only a single set of chromosomes (Forsburg and Rhind, 2006). This is crucial in examining genes of interest in disease models, as mutant alleles can be screened for loss-of-function phenotypes when compared to the wild type alleles (Hoffman et al., 2015). Altogether, the ease of manipulation and the genomic conservation of *S. pombe* makes it a powerful tool to study human disease.

Orthologs of human *TSC1* and *TSC2* genes have been identified in fission yeast (named *tsc1* and *tsc2*, respectively) (Serfontein et al., 2011; Sun et al., 2013). In addition, several components of the mTOR signaling pathway are also conserved in *S. pombe* (Figure 1-4) (Aspuria et al., 2007; Wullschleger et al., 2006). Functional Tsc1p and Tsc2p are crucial in nutrient uptake and the regulation of biosynthetic pathways (Mak and Yeung, 2004). Moreover, the fission yeast Tsc1p-Tsc2p heterodimer regulates a downstream Rheb protein (ortholog of mammalian Rheb) through its GAP activity (Aspuria et al., 2007). As in mammalian cells, Rheb in a GTP-bound state can then activate the *S. pombe* Tor proteins
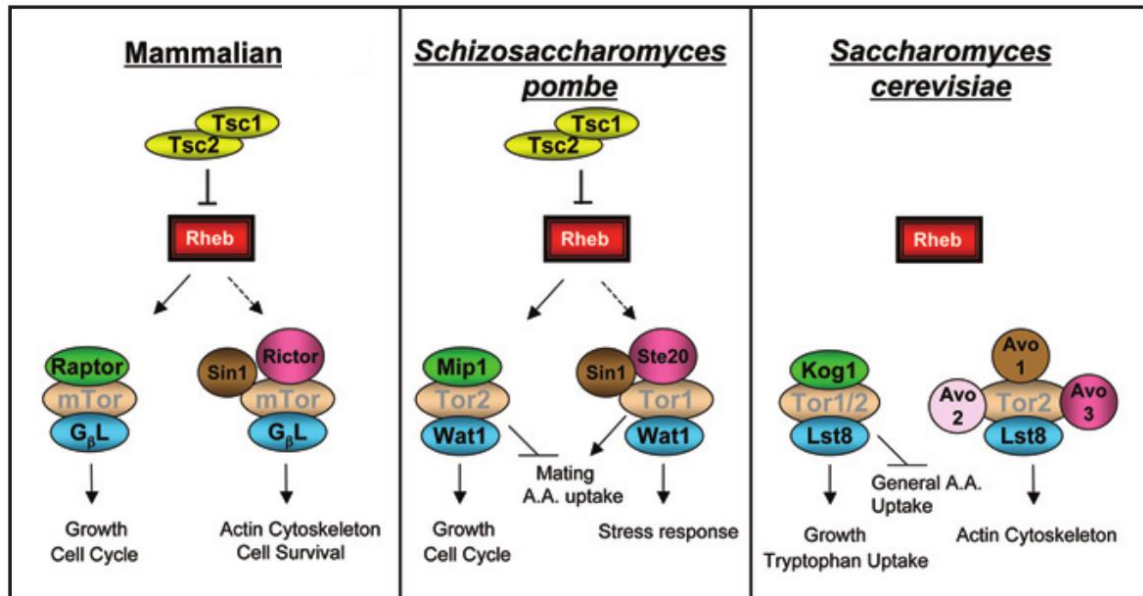
Figure 1-3: The TSC/Rheb/mTOR signaling pathway is well conserved in *S. pombe*. Orthologs of human *TSC1* and *TSC2*, along with several components of the mTOR signaling pathway is conserved in fission yeast. *TSC1* and *TSC2* orthologs do not exist in the budding yeast *Saccharomyces cerevisiae*. Furthermore, *S. pombe* Tor2p forms a complex (with Mip1p and Wat1p) akin to the mammalian mTORC1 to regulate cell cycle and cellular growth. The Tor2p is activated by the upstream Rheb protein which is regulated by the GAP activity of Tsc1p-Tsc2p heterodimer. However, unlike in mammalian cells (Akt phospohorylation of TSC1-TSC2), the upstream regulatory mechanisms of the Tsc1p-Tsc2p complex in fission yeast remain unknown. Proteins with the same color share substantial structural homology across species (i.e. mammalian Raptor, fission yeast Mip1p, and budding yeast Kog1p). Reproduced from Aspuria et al. (2007) under the fair use provision of the Canadian Copyright Modernization Act (2012).

(orthologs of mTOR) (Wullschleger et al., 2006). However, in *S. pombe*, the Tor2p forms the TOR1 complex which interacts in a mTORC1-like manner to regulate protein translation, metabolism and nutrient dependent cellular growth and proliferation (Gonzalez and Rallis, 2017; Matsuo et al., 2007; Rallis et al., 2014). Nonetheless, *S. pombe* is a great adjunct in examining the mechanisms of mammalian TOR signaling and, as such, is important in the understanding of the TSC pathology.

1.4 Gene buffering and genetic interactions

Loss-of-function mutations are crucial in contrasting mutant phenotypes with their respective wild-type phenotypes. In nature, however, these phenotypes are often quantitative and the mechanisms underlying a disease are multifaceted (Hartman IV et al., 2001; Horn et al., 2011). Gene buffering is a phenomena which provides robustness against genetic mutations leading to phenotypic variation and complexity (Kitami and Nadeau, 2002). Classically, gene buffering occurs between genes within the same biological pathway or in parallel pathways with complementary cellular functions (Hartman IV et al., 2001). However, genes in 'redundant' pathways of unrelated biochemical functions can also buffer one another (Kitami and Nadeau, 2002).

Unpredicted phenotypic outcomes resulting from gene buffering between genes are coined as genetic interactions (Costanzo et al., 2011). Recent advances in genome-wide synthetic genetic array (SGA) analysis have allowed for high-throughput identification of these interactions (Collins et al., 2007; Costanzo et al., 2010). Furthermore, digenic (between two genes) interactions can be scored by comparing the fitness of the double mutants – typically colony growth size, against the fitness of the respective single mutants

9

(Baryshnikova et al., 2010; Costanzo et al., 2011; Frost et al., 2012). A digenic genetic interaction is categorized as being either 'positive' or 'negative' in nature (Baryshnikova et al., 2010). Positive interactions occur when the observed double mutant fitness is greater than expected (Costanzo et al., 2011). In contrast, negative interactions occur when double mutant fitness is less than expected (Baryshnikova et al., 2010). Figure 1-5 summarizes the key concepts of gene buffering.

Included in the set of negative interactions are cases of synthetic lethality/sickness (Dixon et al., 2008). In these cases, the simultaneous loss of two gene products results in death or severe growth defects, but the loss of either gene-product individually has little or no effect (Baryshnikova et al., 2013; Costanzo et al., 2011). In tumor cells, synthetic growth defects may also arise between genes and small molecules as a mode of drug discovery; this is because, a typical tumor cell accumulates genetic mutations and morphological changes, exposing the tumor cell to vulnerabilities that a normal cell would not face (Nijman, 2011). Thus, protein products of genes that are synthetic lethal to tumor-forming genetic mutations are ideal candidates for therapeutic targets (Kaelin, 2005). Hartwell et al. (1997) forged this concept of selectively targeting tumor cells to uncover prospective anticancer drugs. The group used yeast gene deletion mutants to screen pharmaceutical inhibitors (Kaelin, 2005). However, technological advances in gene knockdowns using short interfering RNAs (siRNAs) and short hairpin RNAs (shRNAs), and CRISPR/Cas9-mediated complete gene knockouts through guide RNAs (gRNAs) have made it possible to lead high-throughput screens for synthetic lethality across genomes (Beijersbergen et al., 2017). Figure 1-6 highlights the fundamental strategies used with respect to the exploitation of synthetic lethality in uncovering novel cancer therapeutics.
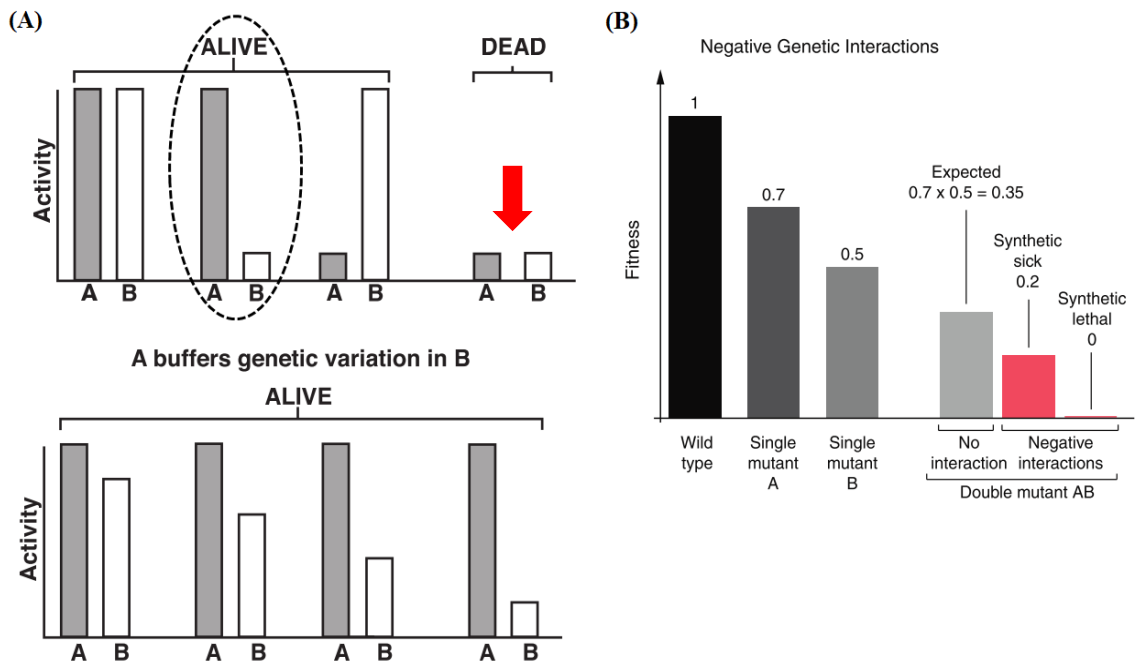
Figure 1-5: The buffering of genetic variation. (A) Phenotypic variation due to gene A is modulated by gene B, and vice versa. The dotted circle (upper panel) highlights the capacity of gene A to "buffer" variation in gene B. This is to say, in the presence of functional gene A, gene B can accumulate genetic variation without affecting its activity (lower panel). Simultaneous mutations in both genes A and B lead to an abrogation of genetic buffering and a lethal phenotype (red arrow). Modified from Hartman IV et al. (2001) under the fair use provision of the Canadian Copyright Modernization Act (2012). **(B)** Negative genetic interactions arise when the double mutant (AB) fitness/phenotype is impaired beyond the expected. The resultant synthetic growth defect can be classified as synthetic sick or synthetic lethal. Modified from Costanzo et al. (2011) under the fair use provision of the Canadian Copyright Modernization Act (2012).

11
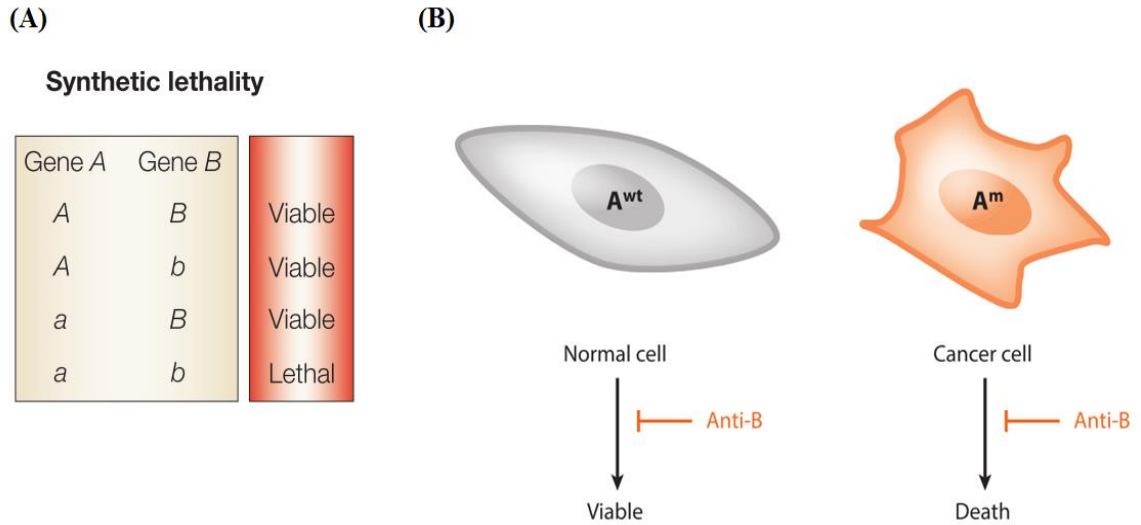
Figure 1-6: Applying synthetic lethality to cancer therapeutics. **(A)** Standalone mutations to either gene A or gene B is tolerated (viable phenotype). However, simultaneous mutation of both genes causes lethality. Reproduced from Kaelin W (2005) under the fair use provision of the Canadian Copyright Modernization Act (2012). **(B)** The tumor cells have acquired a genetic mutation in gene A. Since gene A and B are synthetic lethal, inhibition of gene B or the gene B protein product with an Anti-B agent (gene knockout or pharmacological inhibitor) will lead to tumor-specific cell death. A^{wt} = wild-type gene A, and A^{m} = mutant gene A. Reproduced from Beijerbergen et al. (2016) under the fair use provision of the Canadian Copyright Modernization Act (2012).

Fortunately, these strategies have led to the discovery of numerous drug targets across a variety of cancer models (Beijersbergen et al., 2017; Costa-Cabral et al., 2016; Pourdehnad et al., 2013).

1.5 Genetics to therapeutics: rationale for my study

Inhibition of mTOR signaling with rapamycin has previously shown therapeutic benefits in treating TSC patients; but, rapamycin-independent pathways are also thought to play a role in the manifestation of the disorder (Franz and Weiss, 2012; Kenerson et al., 2005). Furthermore, resistance to rapamycin treatment has been observed in rat models of the disease (Kenerson et al., 2005; Mak and Yeung 2004). Interestingly, combination therapies involving rapamycin and secondary drugs have shown potency in limiting tumorigenesis (Li et al., 2007; Perera et al., 2009). Hence, the identification of alternate 'drugable' targets for novel and/or combination therapies may provide more effective options for the treatment of the TSC pathology (Neuman and Henske, 2011).

Fortunately, recent advances with respect to genetic buffering have provided novel avenues of therapeutic exploration. These avenues rely on the creation of genetic interaction maps, known as genetic interactomes (Costanzo et al., 2011). Genome-wide interactomes and subsequent analyses in budding yeast, *Caenorhabditis elegans*, and mouse fibroblasts, have shown that these interactions can influence a variety of phenotypes associated with complex genetic phenomenon, including human disorders (Baryshnikova et al., 2013). Of particular interest to TSC researchers are negative interactor genes that display synthetic growth defect in conjunction with the *TSC1* or *TSC2* loss of heterozygosity. Inhibiting such genes would presumably impede the growth of

homozygous tumor cells (bearing two mutant copies of the affected TSC gene) while leaving phenotypically normal heterozygous cells unaffected (carrying only the mutant germline copy) (Beijersbergen et al., 2017; Kaelin, 2005). Interestingly, a recent screen for synthetic growth defects in mammalian cells led to the identification of candidate drug targets for the TSC pathology (Housden et al., 2015). Therefore, these negative interactors might represent an "Achilles' heel" of tumor cells deficient in hamartin/tuberin function and, therefore, are ideal targets for therapeutic intervention in TSC patients.

Ryan et al. (2012) recently constructed a large-scale genetic interactome for the fission yeast *S. pombe*. The group has provided an opportunity to test the idea that genetic buffering relationships can indeed be exploited to identify novel drug targets. Using the genetically tractable fission yeast as a model, my study aimed to utilize advances in genetic interaction biology to elucidate the cellular and molecular mechanisms of TSC pathogenesis. In brief, a series of experiments were conducted to address the following areas of interest: (i) the validation of putative negative interactors of fission yeast *tsc1* and *tsc2*, (ii) the identification of sites within these interactors that may be amenable to pharmacological inhibition, (iii) investigation of the fission yeast *tsc2* alleles bearing orthologous mutations to clinical TSC patients, and (iv) the conservation of *S. pombe* synthetic interactions in mammalian cells. Altogether, my study sought to identify novel targets for inhibitory drugs, to be used alone (or in combination with rapamycin) to obstruct tumor-specific growth in individuals affected by the TSC pathology.

1.6 Hypothesis and predictions

I hypothesize that perturbation of the fission yeast negative interactor genes will alter the cellular growth of the *tsc1Δ* and *tsc2Δ* mutants as well as the *tsc2* strains bearing orthologous clinical mutations (i.e. loss of function mutations). Additionally, I predict that complete gene deletions of the validated interactors, or the site-directed mutagenesis within their catalytic sites will result in the impediment of colony growth in *tsc1Δ* and *tsc2Δ* mutant backgrounds. In contrast, I predict that the effect of the mutated interactors in fission yeast cells lacking loss of function mutations of *tsc1* and *tsc2* will be negligible.

Moreover, I hypothesize that the synthetic interactions in *S. pombe* will be conserved in mammalian cells. I predict that RNAi-mediated knockdowns of target genes (orthologous to the validated fission yeast negative interactors) in *TSC2*-deficient mouse fibroblasts will result in cell-specific lethality. I expect such treatments to reduce cellular viability in fibroblasts that match the molecular context of the TSC tumor cells.

CHAPTER II: MATERIALS AND METHODS

2.1 Yeast strains and culture conditions

Fission yeast strains were cultured as indicated in YES, SPA, or EMM media supplemented with a combination of adenine, histidine, leucine, and uracil (Forsburg and Rhind, 2006). Gene deletion strains used in the study were obtained from Bioneer Corporation (https://us.bioneer.com/products/spombe/Library-overview.aspx). Bioneer employs homologous recombination (HR) to replace an ORF of interest with a deletion cassette (Kim et al., 2010). The deletion cassettes are comprised of a *kanMX4* selection marker, which confers resistance to the antibiotic, G418, along with flanking tag sequences and two fragments homologous to the 5' and 3' flanking region of the target ORF (Figure 2-1).

Several *S. pombe* strains bearing site-directed mutations were also constructed. The relevant DNA sequences bearing the desired mutations were synthesized by GenScript® and cloned into the *S. pombe* integration vector, pJK210. The integration constructs were linearized and then transformed into a wild-type strain using the lithium acetate protocol (Gietz et al., 1992). Viable colonies in uracil-deprived EMM-agar media were assessed for integration at the desired locus through colony PCR (Figure 2-2). The products of the colony PCR reactions were analyzed on 1% agarose gels made with tris-acetic EDTA (TAE) buffer and stained with RedSafe™ solution (iNtRON Biotechnology). The genotypes of all *S. pombe* strains used in this study are listed in Table 2-1.
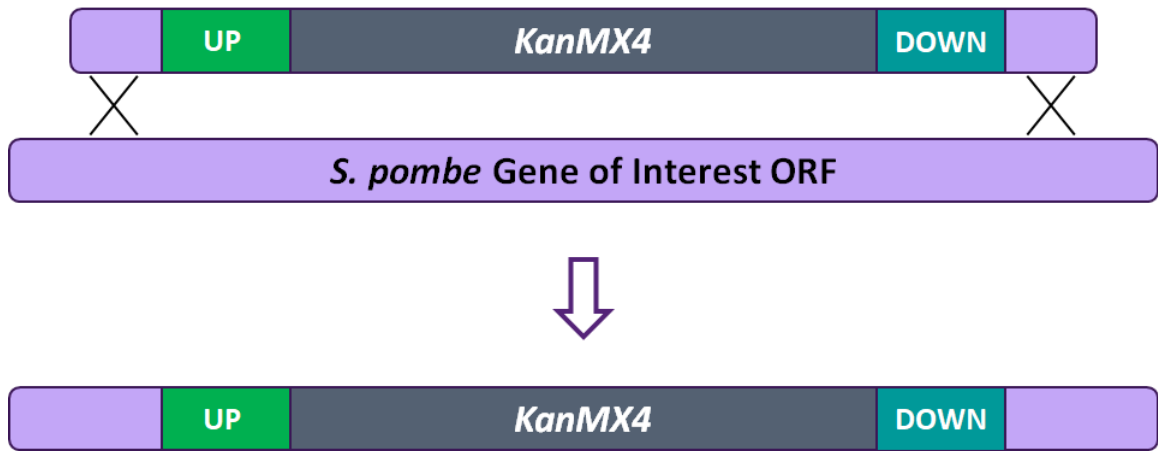
Figure 2-1: Methodology used to construct the Bioneer haploid gene deletion mutant set. Deletion cassettes bearing i) the *kanMX4* marker, ii) flanking tag sequences, and iii) sites of homology to the fission yeast gene of interest were integrated into wild-type *S. pombe* cells via homologous recombination (Kim et al., 2010). Colonies bearing the construct were selected on YES-agar plates supplemented with G418.
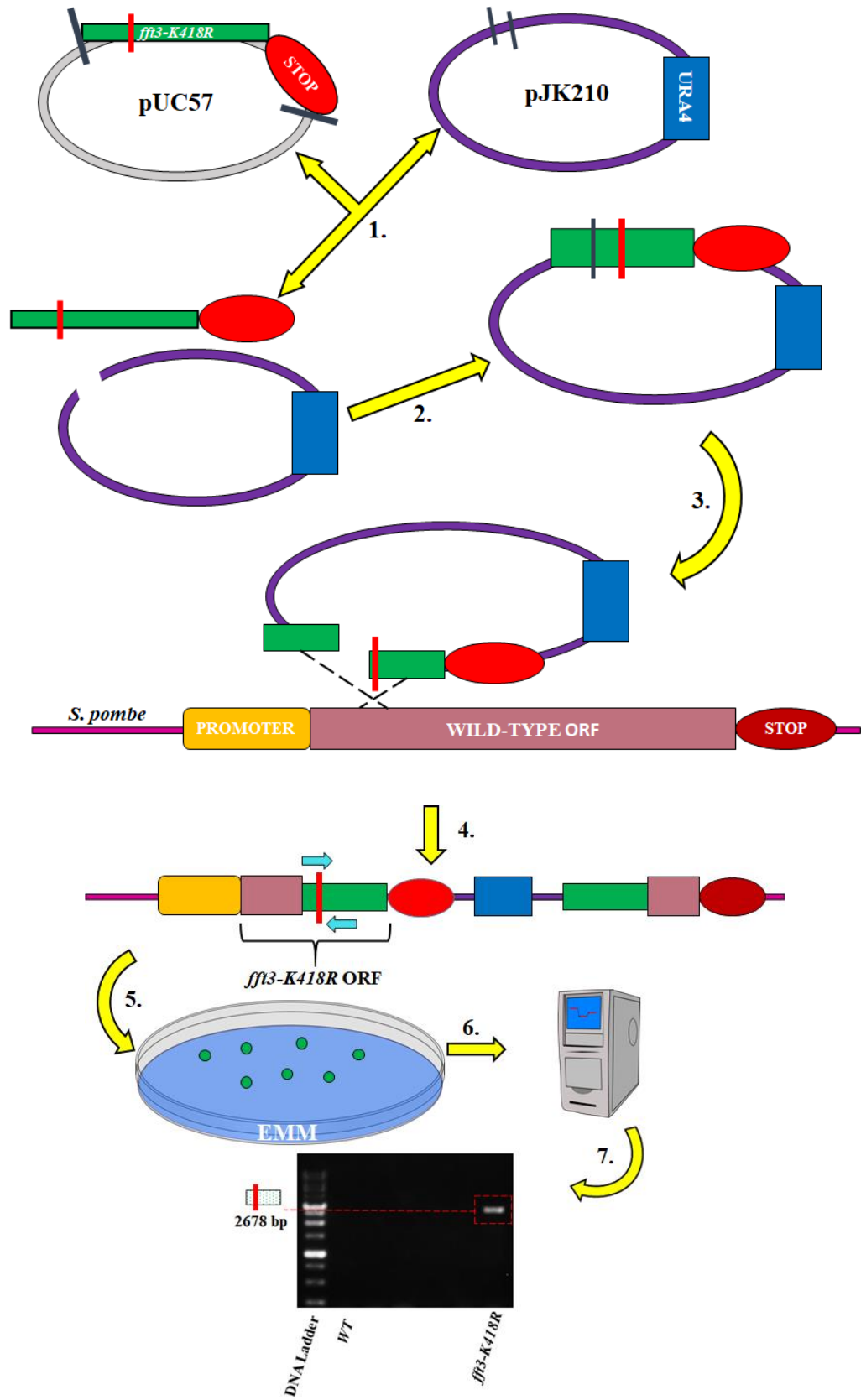
Figure 2-2: Methodology used to generate *ypa1 and fft3* mutant strains via site-directed mutagenesis. The relevant mutant DNA sequences (e.g. to generate the *fft3-K418R* mutant) were designed and ordered from GenScript®. The synthesized sequences arrived cloned into the pUC57 vector. (**1**) The mutant sequence is freed from the pUC57 vector by restriction digestion (digestion site indicated by vertical grey lines). (**2**) The restriction fragment is cloned into the *S. pombe* integrating vector pJK210 via enzymatic ligation. (**3**) The vector is linearized via restriction digestion (digestion site indicated by a vertical grey line). (**4, 5**) The linearized vector is transformed into *S. pombe* where it integrates at the native locus via homologous recombination to generate mutant colonies on uracil-deprived EMM media. (**6, 7**) Integration at the correct locus is verified by colony PCR (2678 bp amplification). Vertical red bars represent the site-directed mutation of Lysine[418] (K418R). Bright teal arrows indicate the primer set used to verify *fft3-K418R* integration into the wild-type fission yeast genome.

Table 2-1. *S. pombe* **strains used in the study.**

Strain	Genotype	Source
JK484	*ura4-D18 leu1-32 ade6-210 his3-D1 h-*	JK collection
ED666	*ura4-D18 leu1-32 ade6-210 h+*	JK collection
UC7	*ura4-D18 h+*	JK collection
UC8	*ura4-D18 h-*	JK collection
TSC13	*tsc1::ura4 ura4-D18 h+*	Bioneer
TSC14	*tsc2::ura4 ura4-D18 h+*	Bioneer
TSC17	*tsc1::ura4 ura4-D18 h-*	JK collection
TSC18	*tsc2::ura4 ura4-D18 h-*	JK collection
TSC83	*ypa1::kanMX4 h+*	Bioneer
TSC86	*fft3::kanMX4 h+*	Bioneer
P17-81	*cdk11::kanMX4 h+*	Bioneer
AR1	*ypa1-D212G::ura4+*	This study
AR2	*ypa1-V208D::ura4+*	This study
AR3	*fft3Δ791-872::ura4+*	This study
AR4	*fft3-K418R::ura4+*	This study
TSC154	*tsc2::tsc2-R1296P h-*	JK collection
NGE1	*lip2::kanMX4 h+*	Bioneer
NGE2	*aap1::kanMX4 h+*	Bioneer
NGE3	*atg14::kanMX4 h+*	Bioneer
NGE4	*spac25a8.03c::kanMX4 h+*	Bioneer

2.2 Generation of *S. pombe* double mutants

Fission yeast double mutants were generated using standard genetic techniques (Forsburg and Rhind, 2006). Briefly, cells of each single mutant strain were mixed on SPA-agar media and incubated at 30°C as mating process is temperature-sensitive. SPA media is nitrogen-deprived and induces mating and sporulation, resulting in tetrads, each comprised of four haploid spores. Once a given cross was plated on a fresh YES-agar plate, a Zeiss Axioskop 40 microscope was utilized to dissect the individual tetrad. Following a brief incubation period at 30°C (to break down tetrad walls), the haploid spores were separated. The individual spores formed colonies within 48 hours and viable double mutants were isolated on YES-agar plates containing G418 antibiotic and/or EMM media lacking uracil.

2.3 Colony growth analysis

The *S. pombe* double mutant strains were streaked onto YES-agar plates along with the respective single gene deletion mutants and a wild-type control. Next, the Zeiss Axioskop 40 microscope was utilized to separate individual cells and arrange them across the YES-agar media (three trials consisting a maximum of four technical replicates from each strain). The plates were incubated at 30°C for five days to assay colony growth. Images were taken every 24 hours using an Alpha Innotech Flurochem SP imaging system. Colony sizes were measured using ImageJ (Abràmoff et al., 2004).

2.4 Cell culture and reagents

Tsc2$^{+/+}$*p53*$^{-/-}$ (P118) and *Tsc2*$^{-/-}$*p53*$^{-/-}$ (P119) mouse embryonic fibroblasts (MEFs) were kindly provided by Dr. DJ Kwiatkowski, Brigham and Women's Hospital, Harvard

Medical School, Boston, MA, USA. These MEFs are connective tissue cells that are precursors to extracellular matrix and collagen, harvested from mouse embryos age embryonic day10.5 (E10.5) (Zhang et al., 2003). The *p53* knockout (*p53*$^{-/-}$) was necessary to prevent premature senescence of the *Tsc2*$^{-/-}$ MEFs (Zhang et al., 2003). All cells were maintained in Dulbecco's modified Eagle's medium (DMEM) supplemented with 10% fetal bovine serum (FBS), 100 IU/mL penicillin, and 100 µg/mL streptomycin (pen-strep). The cells were grown at 37°C in a humidified atmosphere of 5% CO_2 and 95% air up to 70-90% confluency before sub-culturing. P118 and P119 cell cultures were observed and imaged using an inverted Leica DM IL LED microscope in integrated modulation contrast (IMC) mode. DMEM and FBS were purchased from Life Technologies. Pen-strep, DPBS, and TrypLE were obtained from Gibco. Trypan Blue for cell counting was purchased from Sigma-Aldrich. Falcon T-25 and T-75 animal cell culture flasks were used to passage and maintain the MEFs.

2.5 Genotyping the mouse embryonic fibroblasts

The *Tsc2*$^{-/-}$ line was previously generated by inserting a neomycin cassette into exon 3 of the *Tsc2* gene (Figure 2-3) (Onda et al., 1999). To confirm the knockout, genomic DNA (gDNA) was isolated from the P118 and P119 MEFs using DNAzol® (Molecular Research Centre, Inc.). Subsequent PCR reactions were performed using oligonucleotides H162, H163, and H164 (Table 2.2). PCR products were analyzed on 1.7% agarose gel made with TAE buffer and stained with SYBR® safe (Invitrogen).
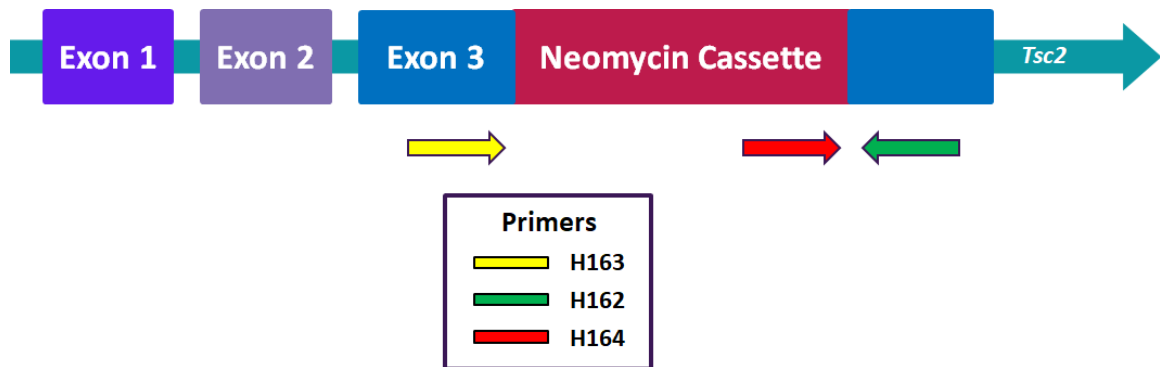
Figure 2-3: Generation of the *Tsc2*^{-/-} allele in mouse embryonic fibroblasts. A neomycin cassette was inserted into exon 3 of the mouse *Tsc2* gene (Onda et al., 1999). This construct disrupted *Tsc2* coding sequence (CDS). Coloured arrows represent the primer binding sites of the oligonucleotides designed to confirm the absence/presence of the neomycin cassette in the P118 and P119 MEFs.

2.6 Transfections

siGENOME SMARTpool siRNAs targeting *Ppp2r4* and *Smarcad1* mouse genes were purchased from Dharmacon™. In addition, a scrambled siRNA targeting no known mouse gene was also obtained. A working concentration of 10 nM was used for each siRNA for transfections. All transfections were done using the Lipofectamine® RNAiMAX transfection reagent (Invitrogen) according to the manufacturer's protocol. Cells were grown to 40-60% confluency in media lacking pen-strep. Transfections were then performed in either 24-well or 96-well plates. Cells were then incubated at 37°C with 5% CO_2 for 48 hours before further assays were performed.

2.7 RNA extraction and cDNA synthesis

Cells were transfected with siRNAs in 24-well plates and incubated for 48 hours. Total RNA was then isolated from transfected cells using TRIzol™ Reagent (Invitrogen) according to the manufacturer's protocol. SuperScript™ III First-Strand Synthesis Supermix for qRT-PCR kit (Invitrogen) was used to generate respective cDNA from 1 µg of total RNA. Subsequent PCR reactions were performed with AR3F and AR3R, AR4F and AR4R, or AR5F and AR5R to confirm gene knockdowns (Table 2-2). PCR products were then analyzed on 1.7% agarose gel made with TAE buffer and stained with SYBR® Safe (Invitrogen).

Table 2-2. Oligonucleotides used in the study. Complete forward (F) and reverse (R) primer sequences along with the size of the PCR products are shown.

Primers	Gene	Sequence (5' to 3')	Amplicon Size
AR1	*ypa1*	F: TACAGCGTCTCAATATTGCATCTG	1024 bp
		R: TCCTATGTTGTGTGGAATTGTGAG	
AR2	*fft3*	F: TCCCTCATTTACTTCCTCTGCTAA	2426 bp (*fft3Δ791-872*) and 2678 bp (*fft3-K418R*)
		R: TCCTATGTTGTGTGGAATTGTGAG	
AR3	*Gapdh*	F: TGGCCTTCCGTGTTCCTAC	178 bp
		R: GAGTTGCTGTTGAAGTCGCA	
AR4	*Ppp2r4*	F: ACCCCTCCAACTACTCAGAAC	215 bp
		R: CACCTATCCAGCGTATCAAGAAG	
AR5	*Smarcad1*	F: TGTTTGCGGAAGATCAAGACG	201 bp
		R: CAGAGTCCTCTACGGCTTTCTTA	
H162/ H163	*Tsc2*	F: ACCCACCTCCTCAAGCTTCT	198 bp
		R: AGACTGCCTTGGGAAAAGCG	
H162/ H164	*Tsc2*	F: ACCCACCTCCTCAAGCTTCT	96 bp
		R: TTGGTTTACAGGGGAAATGC	

2.8 Cell viability assay

The viability of siRNA-transfected cells was evaluated using the CellTiter-Glo$^{\circledR}$ Luminescent Cell Viability Assay (Promega). The assay mobilizes ATP in the viable cells to emit stable luminescent signals that can be measured. The results from the assay estimates metabolically active cells and can be analyzed to determine differences in cell viability among various groups. P118 and P119 MEFs were first seeded at 0.25 x 10^6 cells/mL in 96-well plates (100 µL/well). Cells were then transfected with the relevant siRNAs within a 24 hours incubation period. After a transfection period of 48 hours, 100 µL of the CellTiter-Glo reagent was directly added to the individual wells. The Infinite M1000 (Tecan) monochromator based microplate reader was utilized to quantify the "glow-type" luminescent signals in the 96-well plates.

2.9 Data analysis

Pairwise comparisons of colony sizes were performed among the wild-type, single mutant and the double mutant *S. pombe* strains. Statistically significant differences were determined by the non-parametric Wilcoxon Rank Sum test in R v3.2.2 after applying the Benjamini and Hochberg multiple-testing correction (Benjamini and Hochberg, 1995).

Statistically significant differences between control and siRNA treatment groups in cell viability assays were determined by the non-parametric Friedman test in GraphPad Prism v7.0.2 adjusted with the Benjamini and Hochberg multiple-testing correction (Benjamini and Hochberg, 1995). Graphical illustrations were produced using the GraphPad Prism v7.0.2 software.

26

CHAPTER III: RESULTS

3.1 Validation of candidate negative interactors

Recent high-throughput efforts in *S. pombe* have resulted in the creation of a genetic interaction map (http://interactome-cmp.ucsf.edu/pombe2012/modules/search.html; Ryan et al., 2012). Analysis of this publicly available database revealed a subset of thirteen genes that are negative interactors of both *tsc1* and *tsc2*. This small group of genes displayed strong synthetic growth defects (SGA scores of less than -4) when deleted in combination with *tsc1* or *tsc2* gene deletions. Of these genes, only *ypa1* and *fft3* were selected for validation and detailed analysis as they have clear orthologs in a variety of developmentally complex eukaryotes, including humans (Costelloe et al., 2012; De Virgilio and Loewith, 2006; Durand-Dubief et al., 2012; Goyal and Simanis, 2012; Neves-Costa et al., 2009). Interestingly, a genome wide screen in *Drosophila spp.* also identified the *Pitslre* gene as a negative interactor of the fruit fly genes – *Tsc1* and *Tsc2* (Housden et al., 2015). As this gene is conserved in humans (known as *CDK11*) as well as fission yeast (known as *cdk11*), it was also included in this study.

Crosses of *ypa1Δ, fft3Δ,* and *cdk11Δ* mutants with either *tsc1Δ* or *tsc2Δ S. pombe* strains were performed to generate the respective double mutants. Colony growth analysis was then performed to monitor the growth of individual yeast cells over a period of five days (see Figure 3-1, for an example of *ypa1* mutants). Comparisons were made among cells from the following groups – wild-type *S. pombe*, single gene deletion mutants, and the corresponding double mutants.
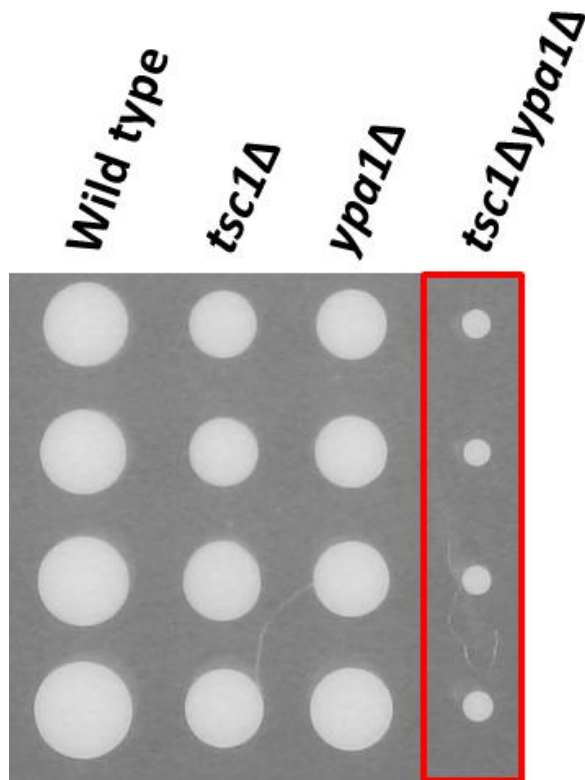
Figure 3-1: Representative example of YES-agar media plate used in colony growth analysis. Several *S. pombe* strains were plated in an YES-agar media plate. Growth was monitored for 5 days. Images were taken at every 24 hours interval. Red box highlights the *tsc1Δypa1Δ* double mutant that exhibits severe growth defect compared to the respective single mutant strains – wild type, *tsc1Δ*, and *ypa1Δ*.

The colony growth analysis revealed that *ypa1Δ* demonstrated strong synthetic growth defects with both *tsc1Δ* and *tsc2Δ* mutants (Figure 3-2). Although, both *tsc1Δ* and *ypa1Δ* single mutant strains were hindered in their ability to grow, the *tsc1Δypa1Δ* double mutant colony sizes were significantly perturbed ($p < 0.0005$ at day 5, for all pairwise comparisons with double mutants; Figure 3-2B). The *tsc2Δypa1Δ* double mutants also followed a similar trend of growth impediment ($p < 0.0005$ at day 5, for all pairwise comparisons with double mutants; Figure 3-2D). In addition, *fft3Δ* mutant demonstrated strong negative interaction with both *tsc1Δ* and *tsc2Δ* mutants ($p < 0.0005$ at day 5, for all pairwise comparisons with double mutants; Figure 3-3 B, D). The resultant colony growth defects of the double mutants (*tsc1Δfft3Δ* and *tsc2Δfft3Δ*) followed similar growth pattern to that of the *tsc1Δypa1Δ* and *tsc2Δypa1Δ* double mutants (Figures 3-2 A, C & 3-3 A, C).

In contrast, the *cdk11* gene deletion mutants did not exhibit any clear growth impediment. The *tsc1Δcdk11Δ* and *tsc2Δcdk11Δ* double mutant colonies were significantly smaller than the wild-type colonies ($p < 0.0005$ at day 5, for all pairwise comparisons with double mutants; Figure 3-4 B, D). However, the double mutant colonies demonstrated similar growth to *tsc1Δ*, *tsc2Δ*, and *cdk11Δ* single mutants ($p > 0.05$ at day 5, for all pairwise comparisons with double mutants; Figure 3-4 A, C). Altogether, *ypa1* and *fft3* were confirmed as negative interactors of both *tsc1* and *tsc2*. As such, the two fission yeast genes were carried forward for further detailed analysis.

3.2 Additional synthetic interaction screens

Recent work in *S. cerevisiae* has indicated that negative interactions can be falsely annotated due to neighboring gene effects (NGEs); whereby, the deletion of a gene can
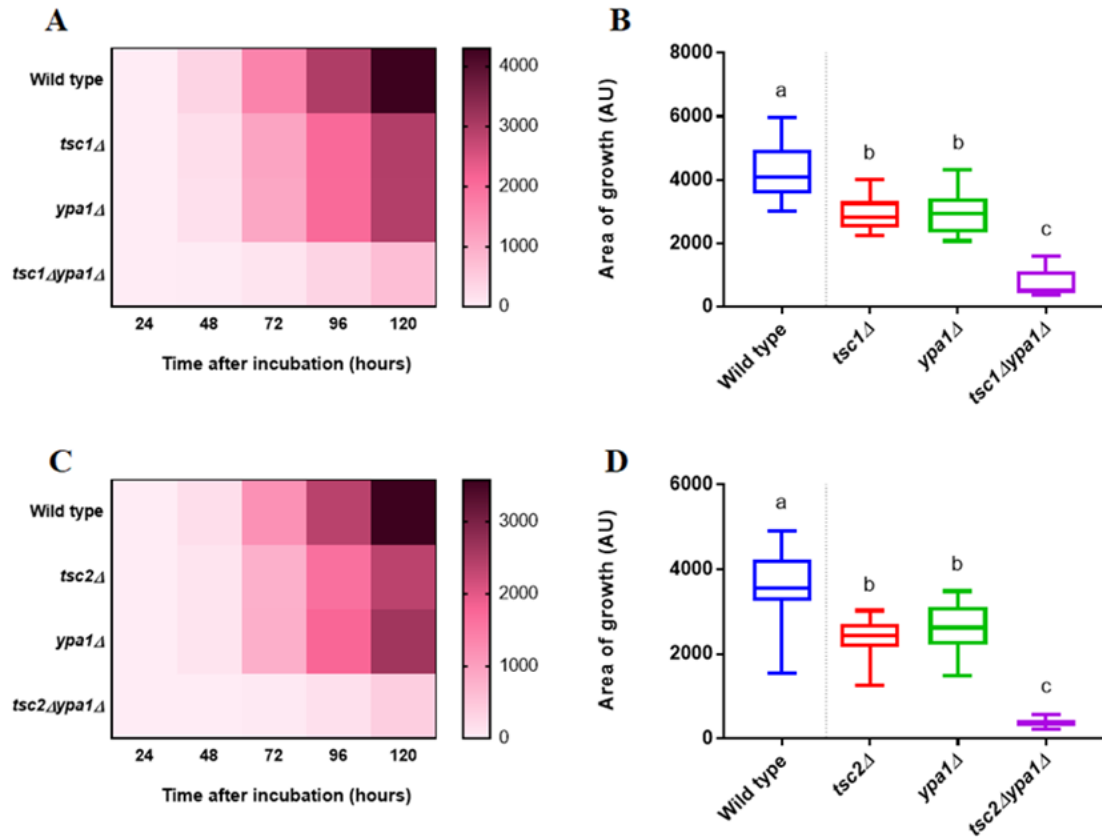
Figure 3-2: *tsc1Δypa1Δ* **and** *tsc2Δypa1Δ* **double mutants exhibit reduced colony growth relative to the respective single mutants.** **(A)** Heat map describing average colony size (arbitrary units) in wild-type, *tsc1Δ*, *ypa1Δ*, and *tsc1Δypa1Δ* mutants over five days ($n = 12$, for all groups). **(B)** Box and whisker plot describing average colony size (arbitrary units) in wild-type, *tsc1Δ*, *ypa1Δ*, and *tsc1Δypa1Δ* mutants at day 5. **(C)** Heat map describing average colony size (arbitrary units) in wild-type, *tsc2Δ*, *ypa1Δ*, and *tsc2Δypa1Δ* mutants over five days ($n = 12$, for all groups). **(D)** Box and whisker plot describing average colony size (arbitrary units) in wild-type, *tsc2Δ*, *ypa1Δ*, and *tsc2Δypa1Δ* mutants at day 5. Lower case letters represent significant differences (if any) among the groups.

Figure 3-3: *tsc1Δfft3Δ* **and** *tsc2Δfft3Δ* **double mutants display decreased colony growth relative to the respective single mutants.** **(A)** Heat map describing average colony size (arbitrary units) in wild-type, *tsc1Δ*, *fft3Δ*, and *tsc1Δfft3Δ* mutants over five days (*n* = 12, for all groups). **(B)** Box and whisker plot describing average colony size (arbitrary units) in wild-type, *tsc1Δ*, *fft3Δ*, and *tsc1Δfft3Δ* mutants at day 5. **(C)** Heat map describing average colony size (arbitrary units) in wild-type, *tsc2Δ*, *fft3Δ*, and *tsc2Δfft3Δ* mutants over five days (*n* = 12, for all groups). **(D)** Box and whisker plot describing average colony size (arbitrary units) in wild-type, *tsc2Δ*, *fft3Δ*, and *tsc2Δfft3Δ* mutants at day 5. Lower case letters represent significant differences (if any) among the groups.
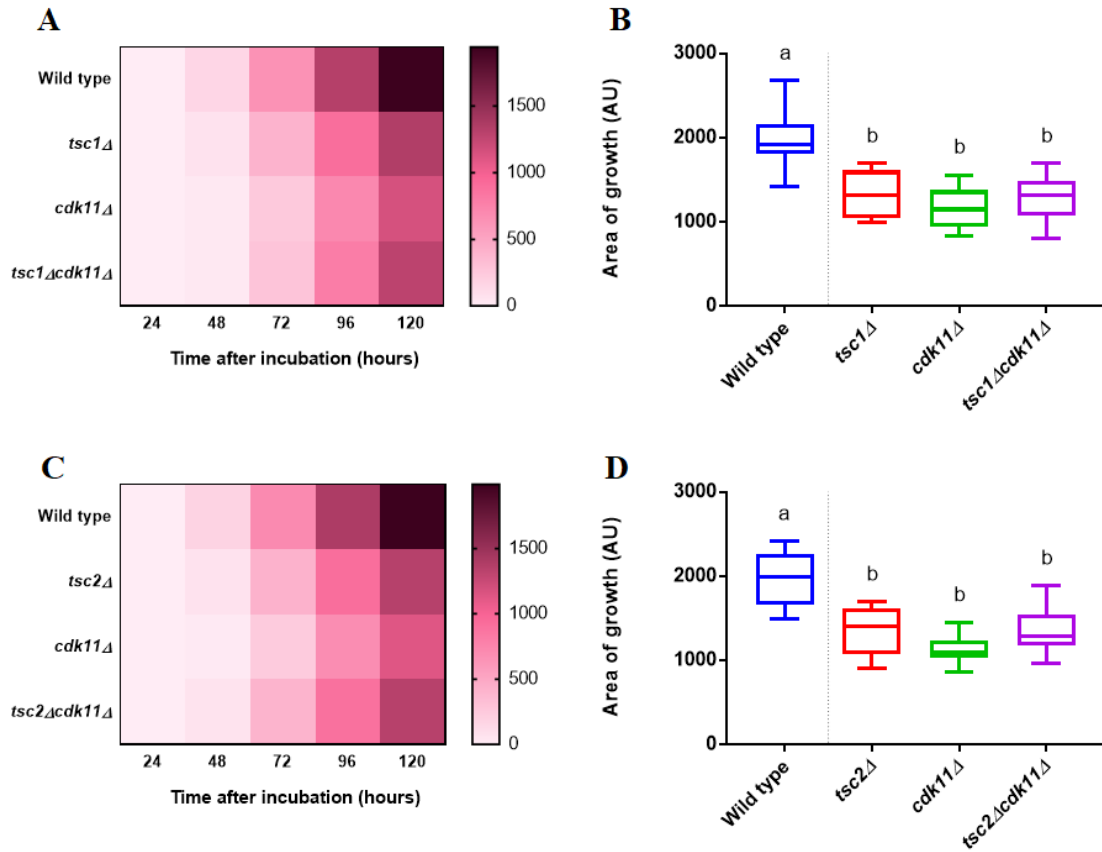
Figure 3-4: *tsc1Δcdk11Δ* and *tsc21Δcdk11Δ* double mutants do not exhibit differences in colony growth relative to the respective single mutants. (A) Heat map describing average colony size (arbitrary units) in wild-type, *tsc1Δ*, *cdk11Δ*, and *tsc1Δcdk11Δ* mutants over five days (*n* = 11, 12, 12, and 12, respectively). **(B)** Box and whisker plot describing average colony size (arbitrary units) in wild-type, *tsc1Δ*, *cdk11Δ*, and *tsc1Δcdk11Δ* mutants at day 5. **(C)** Heat map describing average colony size (arbitrary units) in wild-type, *tsc2Δ*, *cdk11Δ*, and *tsc2Δcdk11Δ* mutants over five days (*n* = 12, for all groups). **(D)** Box and whisker plot describing average colony size (arbitrary units) in wild-type, *tsc2Δ*, *cdk11Δ*, and *tsc2Δypa1Δ* mutants at day 5. Lower case letters represent significant differences (if any) among the groups.

affect the adjacent genes along a genome leading to improper annotation of negative interactions (Atias et al., 2015). In fact, NGE is relatively extensive with a ~10% rate, which can distort large-scale genetic interactomes (Ben-Shitrit et al., 2012). As such, inappropriate recordings of genetic interactions require correction and subsequent replacement with new and correct mapping of the relevant interactions. I examined potential NGE effects on the observed data using the following mutants – *lip2Δ*, *aap1Δ*, *atg14Δ*, and *spac25a8.03cΔ*. These genes are immediately adjacent to the previously validated *tsc1* and *tsc2* negative interactors, *ypa1* and *fft3*. The data demonstrated that the corresponding double mutants of the adjacent gene deletion mutants do not exhibit any significant growth defects compared to the single mutants ($p > 0.05$ at day 5, for all pairwise comparisons with double mutants; Figure 3-5 & 3-6). These results provide strong evidence that the synthetic interactions mapped in this study are not influenced by NGEs.

3.3 Identification of catalytic sites within the interactors

The determination of specific functional domains within Ypa1p and Fft3p can help identify sites that may be amenable to pharmacological inhibitors. Based on current literature and bioinformatic analyses, three domains were identified – one within the Ypa1p (PPIase domain) (Jordens et al., 2006; Jouvet et al., 2011; Leulliot et al., 2006), and two within the Fft3p (ATPase domain and helicase domain) (Byeon et al., 2013; Chen et al., 2012; Eapen et al., 2012; Steglich et al., 2015). An online based multi-alignment tool, Clustal Omega (Sievers et al., 2011), was used to verify the conservation of these putative sites across several eukaryotes (Figure 3-7). Using this information, several integration constructs were designed to create *S. pombe* strains expressing *ypa1-D212G*, *ypa1-V208D, fft3-K418R*, and
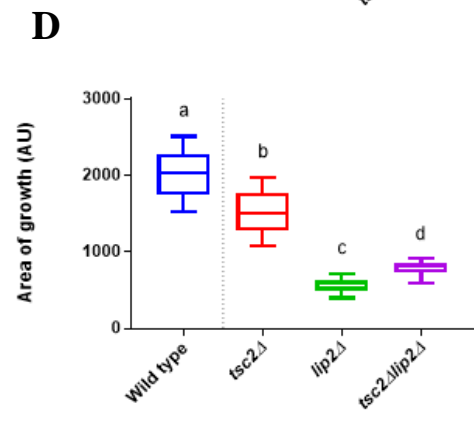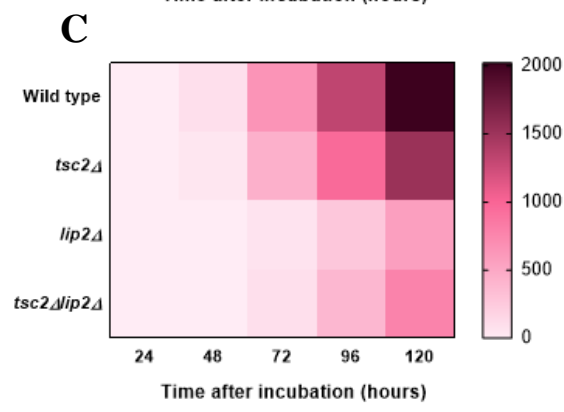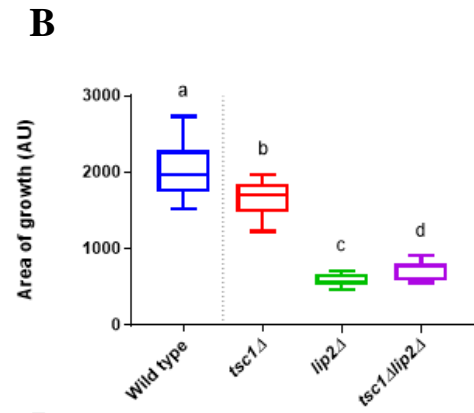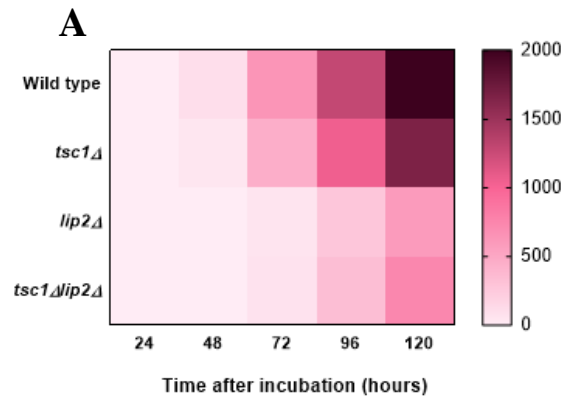
Figure 3-5: Double mutants of *lip2Δ* and *aap1Δ* (adjacent to *ypa1*) do not exhibit colony growth defects relative to the respective single mutants. (A, C) Heat map describing average colony size (arbitrary units) in wild-type, *tsc1Δ*, *tsc2Δ*, *lip2Δ*, *tsc1Δlip2Δ*, and *tsc2Δlip2Δ* mutants over five days (*n* = 12, 11, 12, 12, 11, and 11, respectively). **(B, D)** Box and whisker plot describing average colony size (arbitrary units) in wild-type, *tsc1Δ*, *tsc2Δ*, *lip2Δ*, *tsc1Δlip2Δ*, and *tsc2Δlip2Δ* mutants at day 5. **(E, G)** Heat map describing average colony size (arbitrary units) in wild-type, *tsc1Δ*, *tsc2Δ*, *aap1Δ*, *tsc1Δaap1Δ*, and *tsc2Δaap1Δ* mutants over five days (*n* = 12, 12, 12, 12, 10, and 12, respectively). **(F, H)** Box and whisker plot describing average colony size (arbitrary units) in wild-type, *tsc1Δ*, *tsc2Δ*, *aap1Δ*, *tsc1Δaap1Δ*, and *tsc2Δaap1Δ* mutants at day 5. Lower case letters represent significant differences (if any) among the groups.

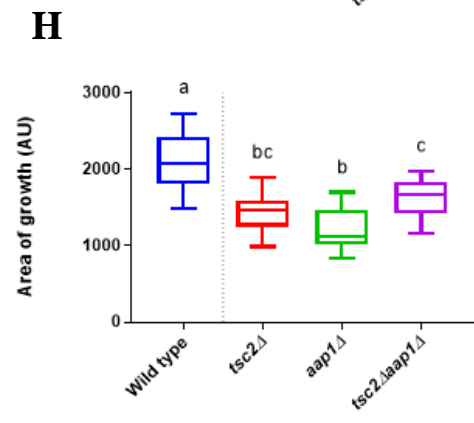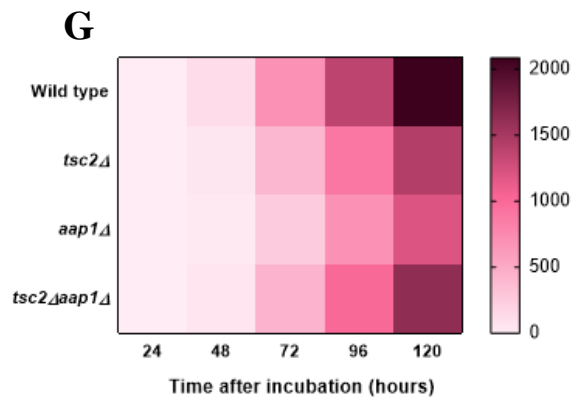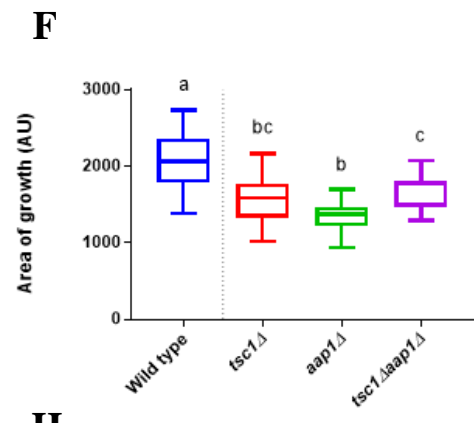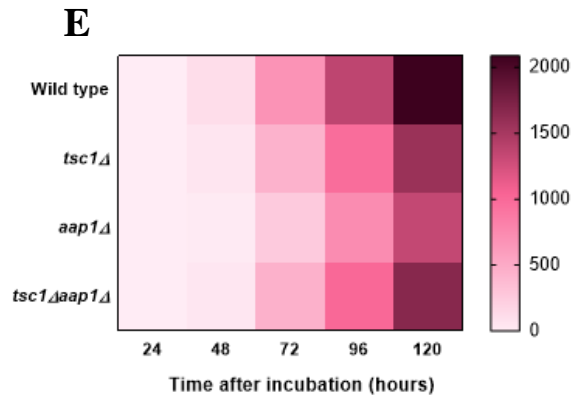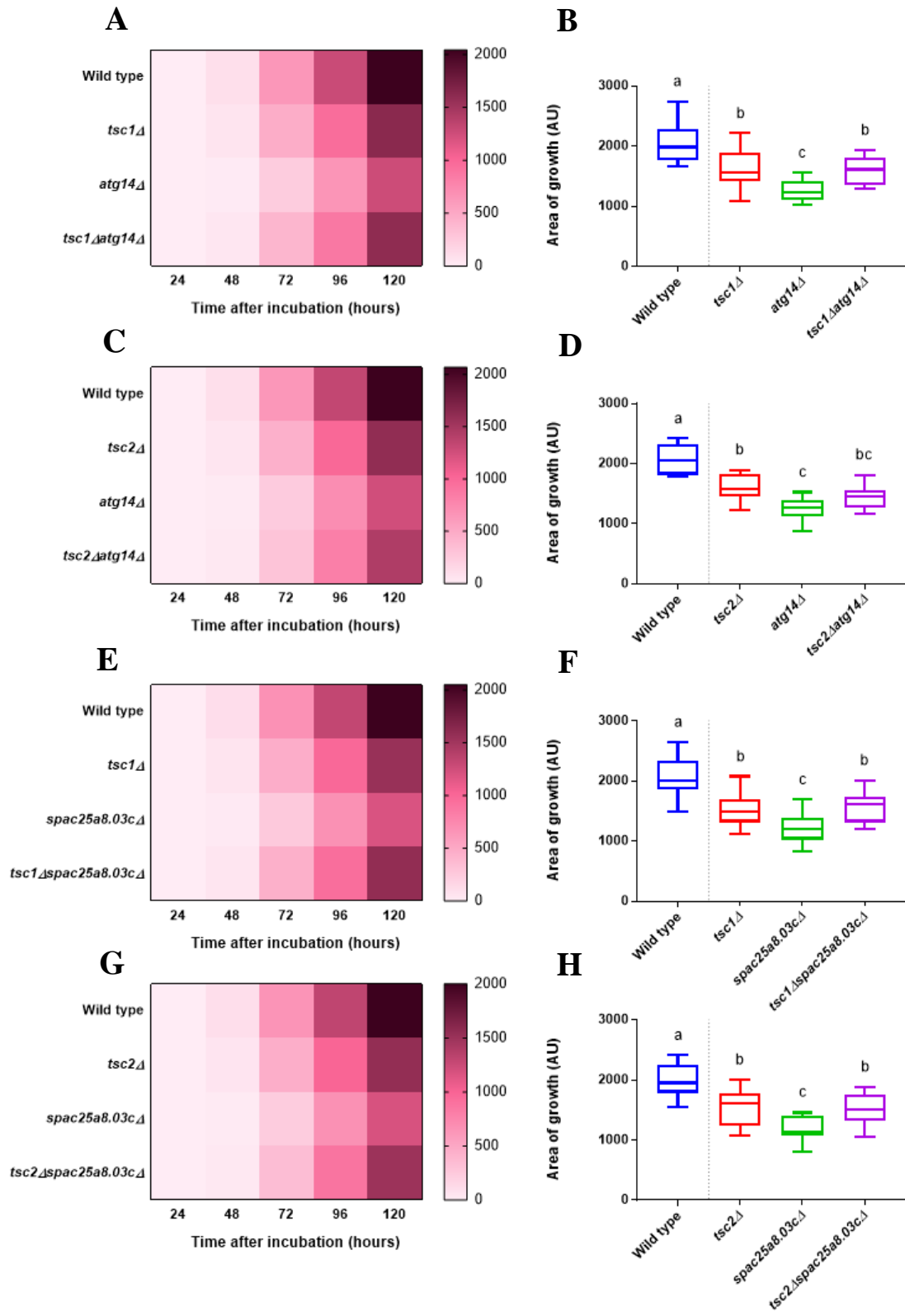**Figure 3-6: Double mutants of *atg14Δ* and *spac25a8.03cΔ* (adjacent to *fft3*) do not exhibit colony growth defects relative to the respective single mutants. (A, C)** Heat map describing average colony size (arbitrary units) in wild-type, *tsc1Δ*, *tsc2Δ*, *atg14Δ*, *tsc1Δatg14Δ*, and *tsc2Δatg14Δ* mutants over five days (n = 12, 11, 12, 11, 8, and 11, respectively). **(B, D)** Box and whisker plot describing average colony size (arbitrary units) in wild-type, *tsc1Δ*, *tsc2Δ*, *atg14Δ*, *tsc1Δatg14Δ*, and *tsc2Δatg14Δ* mutants at day 5. **(E, G)** Heat map describing average colony size (arbitrary units) in wild-type, *tsc1Δ*, *tsc2Δ*, *spac25a8.03cΔ*, *tsc1Δspac25a8.03cΔ*, and *tsc2Δspac25a8.03cΔ* mutants over five days (n = 12, 11, 12, 11, 12, and 12, respectively). **(F, H)** Box and whisker plot describing average colony size (arbitrary units) in wild-type, *tsc1Δ*, *tsc2Δ*, *spac25a8.03cΔ*, *tsc1Δspac25a8.03cΔ*, and *tsc2Δ spac25a8.03cΔ* mutants at day 5. Lower case letters represent significant differences (if any) among the groups.
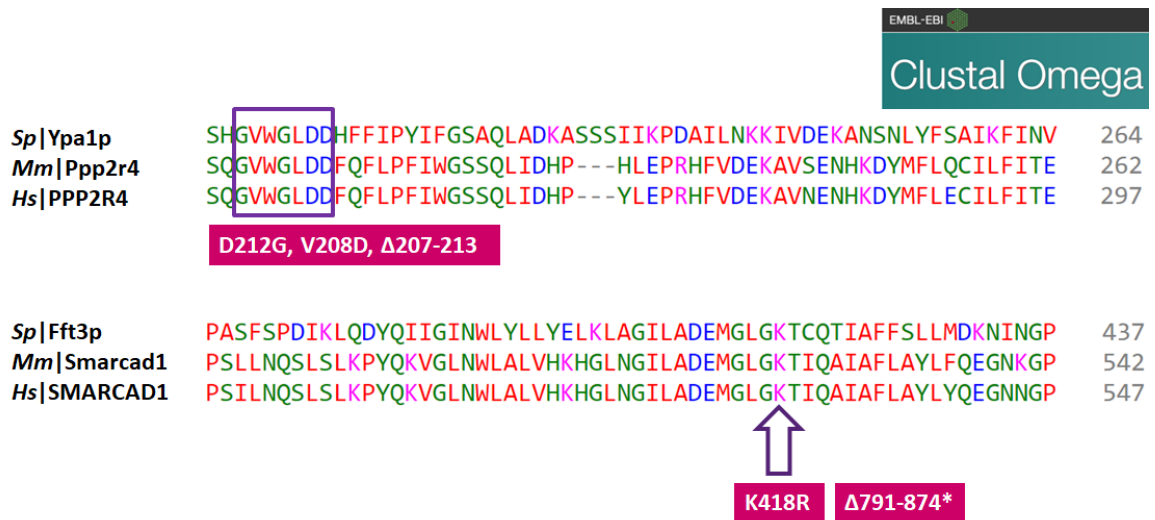
Figure 3-7: Multiple sequence alignments comparing Ypa1p and Fft3p to their human and mouse orthologs. A Highly conserved PPIase domain is present within Ypa1p (purple box). The Fft3p contains a highly conserved ATPase domain (purple arrow) and a helicase domain (*not shown). The pink letter boxes denote the site-directed mutagenesis of fission yeast strains performed in this study. *Sp*, *Schizosaccharomyces pombe*; *Mm*, *Mus musculus*; *Hs*, *Homo sapiens*.

fft3Δ791-874 (see Materials and Methods). The mutant strains were then crossed to either

tsc1Δ or *tsc2Δ* strains to generate the respective double mutants.

The *ypa1* site-directed double mutants (*tsc1Δypa1-D212G*, *tsc2Δypa1-D212G*, *tsc1Δypa1-V208D*, and *tsc2Δypa1-V208D*) did not show any significant differences in colony growth compared to their respective *tsc1Δ* and *tsc2Δ* mutant strains ($p > 0.05$ for all pairwise comparisons at day 5; Figure 3-8 & Figure 3-9). Likewise, the helicase-deleted *fft3* double mutants also followed the growth trends of the *tsc1Δ* and *tsc2Δ* mutants ($p >$ 0.05 for the pairwise comparisons at day 5; Figure 3-10). In contrast, *fft3-K418R* double mutants did show a significant impediment in colony growth compared to the wild-type and respective single mutant strains ($p < 0.05$ for all pairwise comparisons at day 5; Figure 3-11). However, the synthetic growth defects witnessed in these double mutants were not as prominent as the growth defects previously seen in the *fft3Δ* double mutants. Nonetheless, the result suggest that the ATPase domain within the Fft3p may be pharmacologically targeted in cells with loss of function mutations in *tsc1* and *tsc2*.

3.4 Assaying clinically orthologous mutations in *S. pombe*

As part of an ongoing project in the lab, strains expressing *tsc2* alleles bearing mutations orthologous to those found clinically have been created (G296E, R927W, N1191K, N1199S, P1223L, R1296P) (Figure 3-12). These *tsc2* alleles were examined to screen any negative interactions with *fft3* and *ypa1*. Of the six mentioned *tsc2* mutants, only *tsc2-R1296P* mutants were found to negatively interact with both *ypa1* and *fft3* ($p < 0.05$ for all double mutant pairwise comparisons at day 5; Figure 3-13 A to D; data not shown for the other five mutants). Furthermore, the growth defects exhibited by the *tsc2-R1296P ypa1Δ*
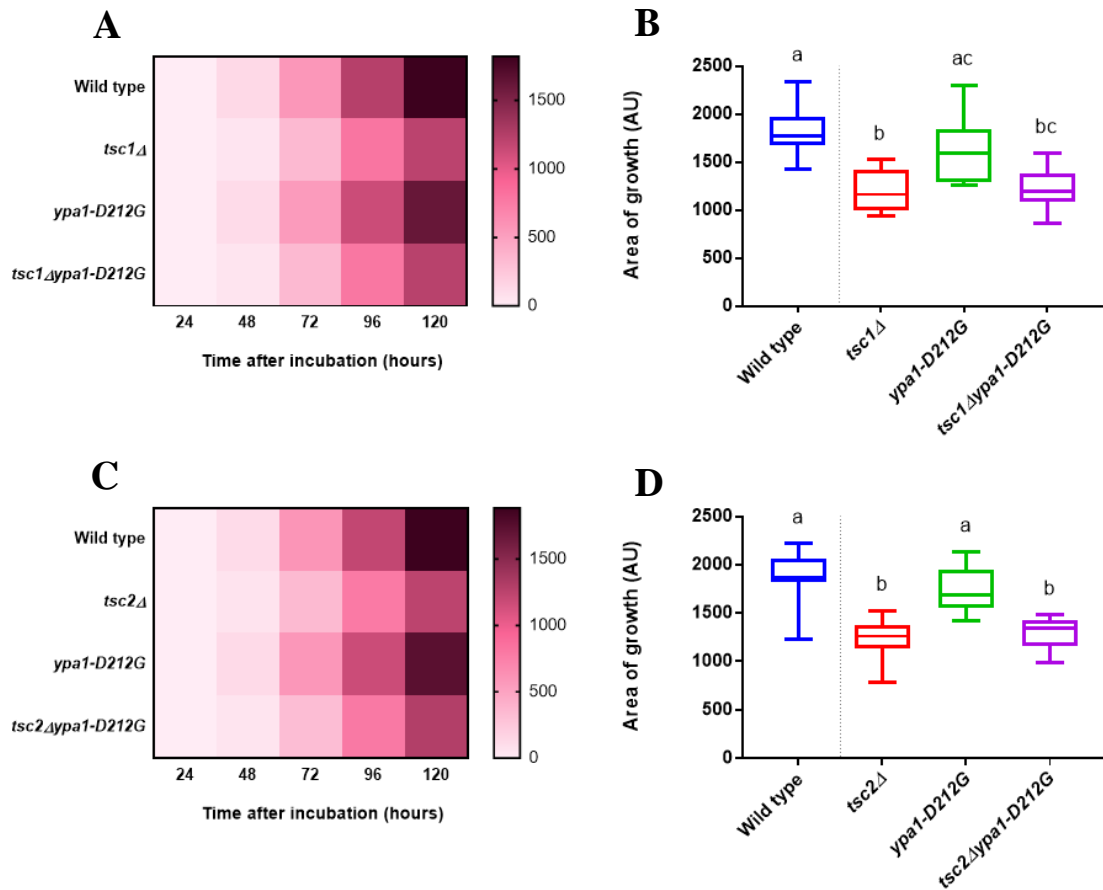
Figure 3-8: *tsc1Δypa1-D212G* and *tsc2Δypa1-D212G* double mutants do not exhibit reduced colony growth relative to the respective single mutants. (**A**) Heat map describing average colony size (arbitrary units) in wild-type, *tsc1Δ*, *ypa1-D212G*, and *tsc1Δypa1-D212G* mutants over five days (*n* = 12, 12, 11, and 12, respectively). (**B**) Box and whisker plot describing average colony size (arbitrary units) in wild-type, *tsc1Δ*, *ypa1-D212G*, and *tsc1Δypa1-D212G* mutants at day 5. (**C**) Heat map describing average colony size (arbitrary units) in wild-type, *tsc2Δ*, *ypa1-D212G*, and *tsc2Δypa1-D212G* mutants over five days (*n* = 12, 12, 12, and 11, respectively). (**D**) Box and whisker plot describing average colony size (arbitrary units) in wild-type, *tsc2Δ*, *ypa1-D212G*, and *tsc2Δypa1-D212G* mutants at day 5. Lower case letters represent significant differences (if any) among the groups.
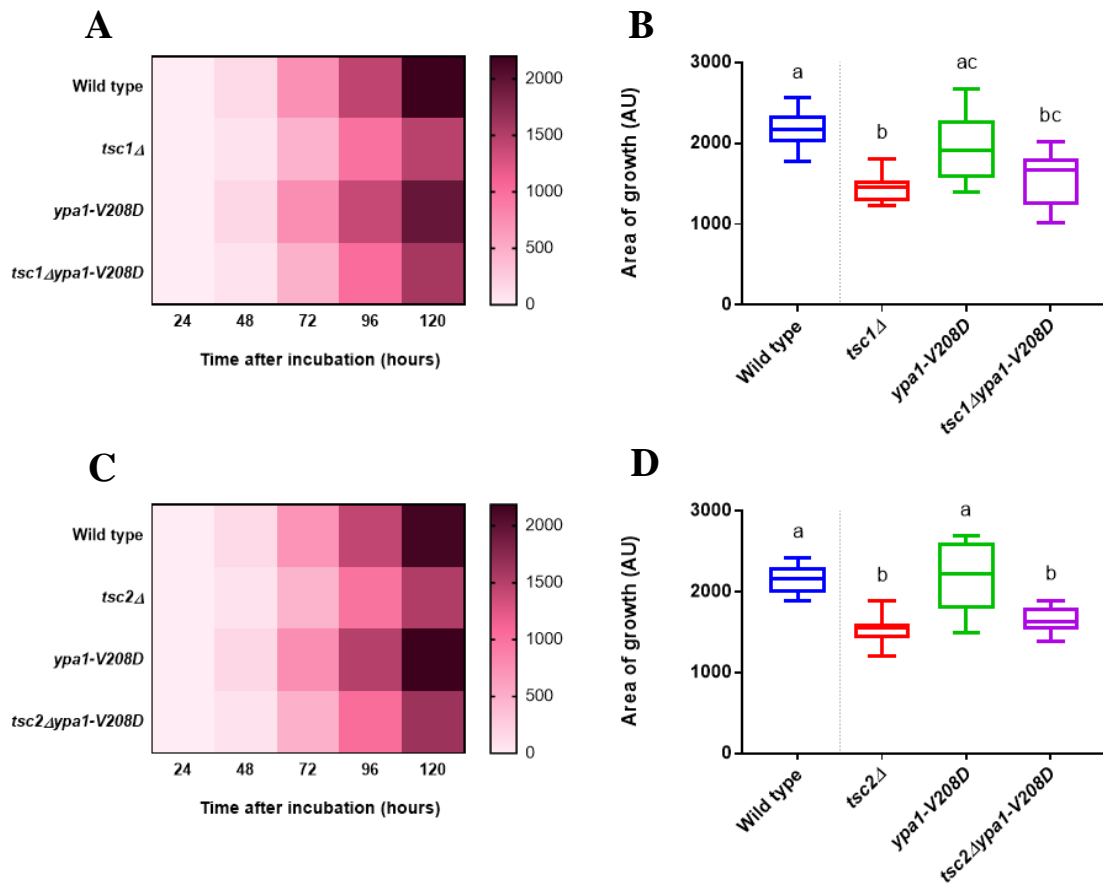
Figure 3-9: *tsc1Δypa1-V208D* **and** *tsc2Δypa1-V208D* **double mutants do not exhibit reduced colony growth relative to the respective single mutants.** (**A**) Heat map describing average colony size (arbitrary units) in wild-type, *tsc1Δ*, *ypa1-V208D*, and *tsc1Δypa1-V208D* mutants over five days (n = 11, 12, 12, and 11, respectively). (**B**) Box and whisker plot describing average colony size (arbitrary units) in wild-type, *tsc1Δ*, *ypa1-V208D*, and *tsc1Δypa1-V208D* mutants at day 5. (**C**) Heat map describing average colony size (arbitrary units) in wild-type, *tsc2Δ*, *ypa1-V208D*, and *tsc2Δypa1-V208D* mutants over five days (n = 12, 12, 10, and 11, respectively). (**D**) Box and whisker plot describing average colony size (arbitrary units) in wild-type, *tsc2Δ*, *ypa1-V208D*, and *tsc2Δypa1-V208D* mutants at day 5. Lower case letters represent significant differences (if any) among the groups.
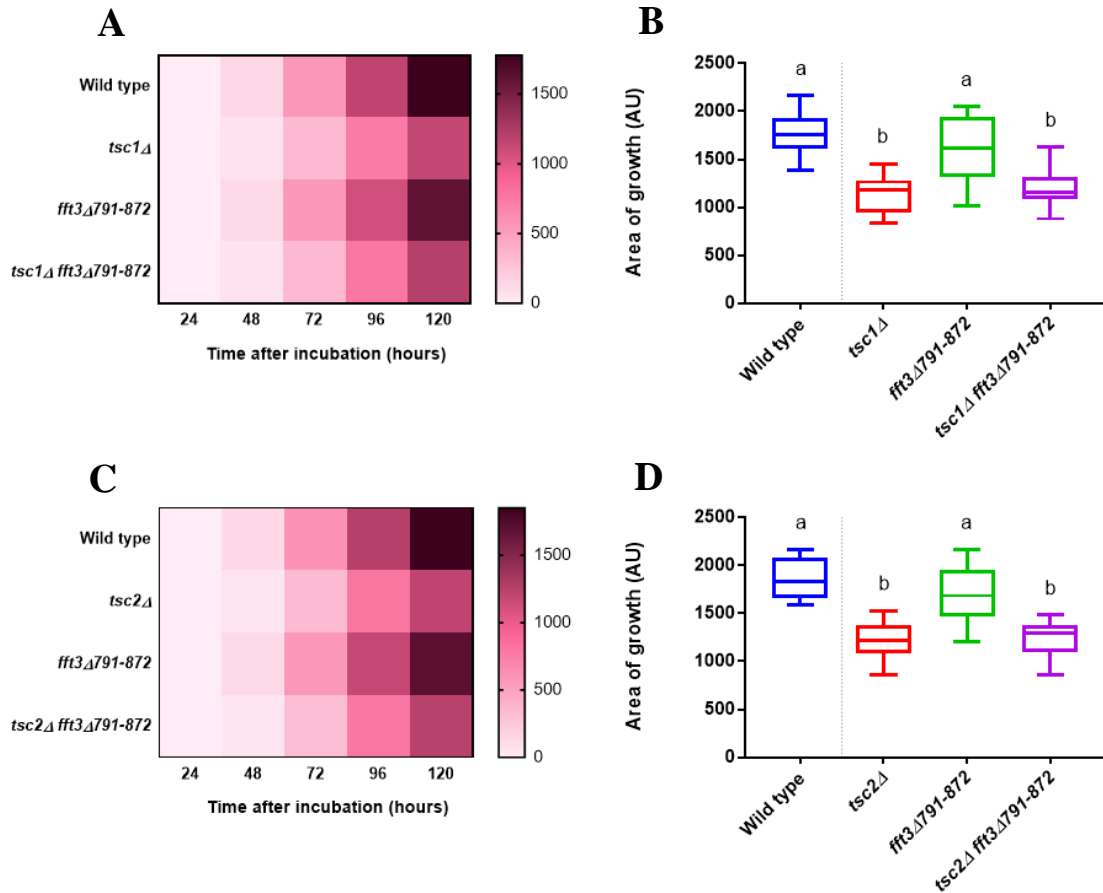
Figure 3-10: *tsc1Δfft3Δ791-872* **and** *tsc2Δfft3Δ791-872* **double mutants do not exhibit reduced colony growth relative to the respective single mutants. (A)** Heat map describing average colony size (arbitrary units) in wild-type, *tsc1Δ*, *fft3Δ791-872* and *tsc1Δfft3Δ791-872* mutants over five days (n = 12, 12, 12, and 11, respectively). **(B)** Box and whisker plot describing average colony size (arbitrary units) in wild-type, *tsc1Δ*, *fft3Δ791-872*, and *tsc1Δfft3Δ791-872* mutants at day 5. **(C)** Heat map describing average colony size (arbitrary units) in wild-type, *tsc2Δ*, *fft3Δ791-872*, and *tsc2Δfft3Δ791-872* mutants over five days (n = 12, for all groups). **(D)** Box and whisker plot describing average colony size (arbitrary units) in wild-type, *tsc2Δ*, *fft3Δ791-872*, and *tsc2Δfft3Δ791-872* mutants at day 5. Lower case letters represent significant differences (if any) among the groups.

Figure 3-11: *tsc1Δfft3-K418R* **and** *tsc2Δfft3-K418R* **double mutants demonstrate reduced colony growth relative to the respective single mutants. (A)** Heat map describing average colony size (arbitrary units) in wild-type, *tsc1Δ*, *fft3-K418R*, and *tsc1Δfft3-K418R* mutants over five days (*n* = 12, 11, 12, and 11, respectively). **(B)** Box and whisker plot describing average colony size (arbitrary units) in wild-type, *tsc1Δ*, *fft3-K418R*, and *tsc1Δfft3-K418R* mutants at day 5. **(C)** Heat map describing average colony size (arbitrary units) in wild-type, *tsc2Δ*, *fft3-K418R*, and *tsc2Δfft3-K418R* mutants over five days (*n* = 12, 11, 12, and 12, respectively). **(D)** Box and whisker plot describing average colony size (arbitrary units) in wild-type, *tsc2Δ*, *fft3-K418R*, and *tsc2Δfft3-K418R* mutants at day 5. Lower case letters represent significant differences (if any) among the groups.
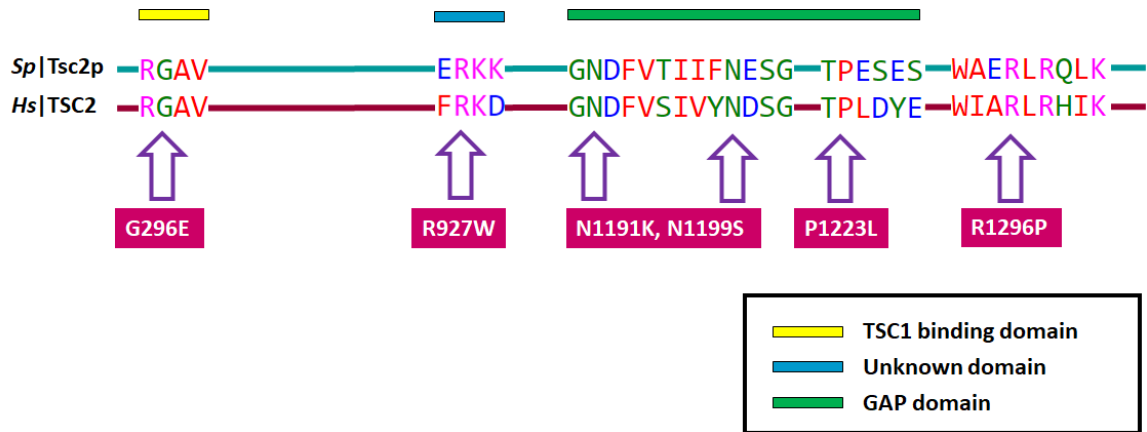
Figure 3-12: Clustal Omega alignment of human TSC2 and fission yeast Tsc2p.
Colored bars indicate domains of the human TSC2 protein that are conserved in *S. pombe* Tsc2p. Pink labelled boxes indicate fission yeast Tsc2p mutations that are orthologous to the corresponding disease-causing human *TSC2* alleles. *Sp*, *Schizosaccharomyces pombe*; *Hs*, *Homo sapiens*.

and *tsc2-R1296P fft3Δ* double mutants were highly comparable to those of the *tsc2Δypa1Δ* and *tsc2Δfft3Δ* double mutants (Figure 3-13 E, F). Thus, the observed interactions between *tsc2* and *ypa1* or *fft3* are indeed allele specific. This demonstrates that the loss of *fft3* or *ypa1* activity is not necessarily detrimental to growth in all cells exhibiting deficiencies in hamartin or tuberin function. Instead, the results imply that the genetic interactions depend on the subtleties of Tsc1p/Tsc2p molecular function in an allele specific manner (see Discussion).

3.5 Genotyping the mouse embryonic cell lines

The validated interactors from the initial screen in *S. pombe* have clear orthologs in organisms ranging from yeast to humans. Thus, *Ppp2r4* (ortholog of *ypa1*) and *Smarcad1* (ortholog of *fft3*) were tested to see if the negative interactions were conserved in more developmentally complex eukaryotes. To this end, $Tsc2^{+/+}p53^{-/-}$ *and* $Tsc2^{-/-}p53^{-/-}$ mouse embryonic fibroblasts (MEFs) were obtained from Dr. DJ Kwiatkowski (Onda et al., 1999).

After the initial thawing process, the P118 ($Tsc2^{+/+}p53^{-/-}$) and P119 ($Tsc2^{-/-}p53^{-/-}$) MEFs were sub-cultured twice before genotyping. Cells show typical fibroblastic morphology (Figure 3-14 A, B) as reported earlier (Onda et al., 1999). For each type of cells, gDNA was isolated and two simultaneous PCR reactions were performed using one of either H163 (within exon 3 of *Tsc2*) or H164 primers (within the neomycin cassette insert) in combination with the H162 primer (within exon 3 of *Tsc2*). Results show an expected 198 base pairs (bp) PCR amplificon for the P118 MEFs (PCR product of H163/H162), with no PCR product from H164/H162 (Figure 3-14 C). In contrast, there was a H164/H162-96 bp PCR product amplified for the P119 MEFs, with no PCR product
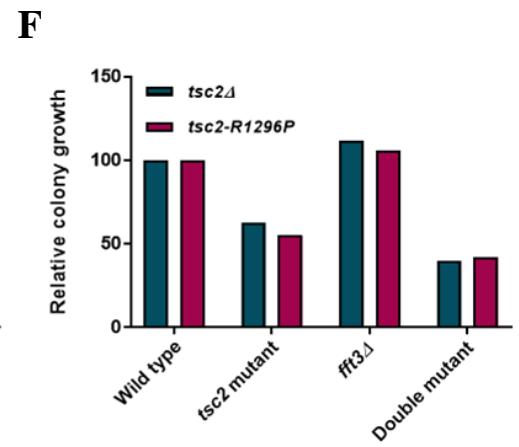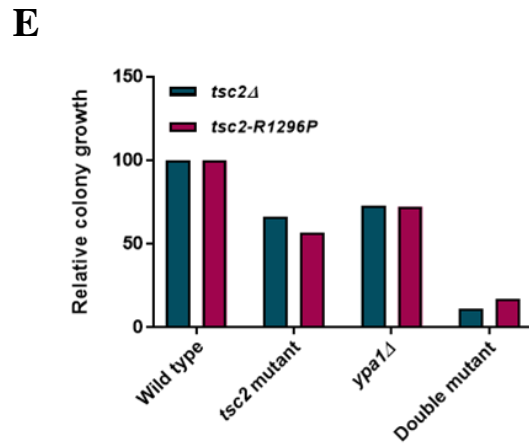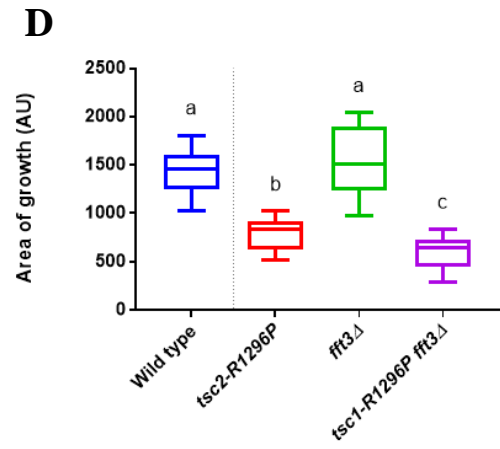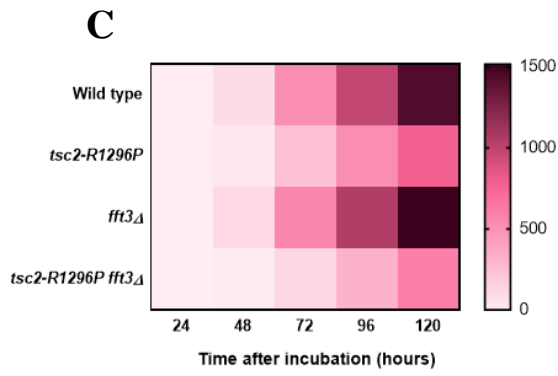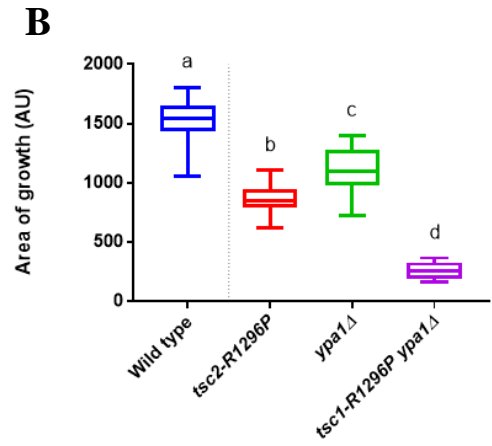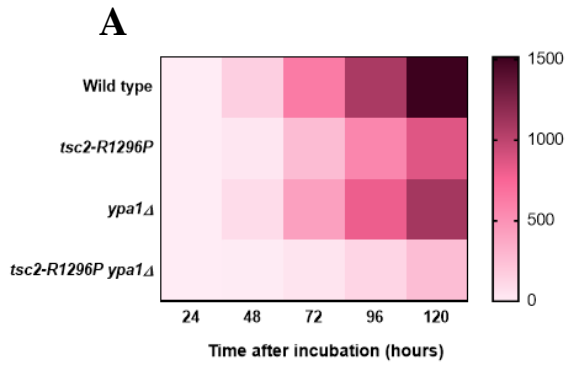
Figure 3-13: *tsc2-R1296P ypa1Δ* **and** *tsc2-R1296P fft3Δ* **double mutants demonstrate reduced colony growth relative to the respective single mutants. (A)** Heat map describing average colony size (arbitrary units) in wild-type, *tsc2-R1296P*, *ypa1Δ*, and *tsc2-R1296P ypa1Δ* mutants over five days ($n = 8, 8, 8$, and 6, respectively). **(B)** Box and whisker plot describing average colony size (arbitrary units) in wild-type, *tsc2-R1296P*, *ypa1Δ*, and *tsc2-R1296P ypa1Δ* mutants at day 5. **(C)** Heat map describing average colony size (arbitrary units) in wild-type, *tsc2-R1296P*, *fft3Δ*, and *tsc2-R1296P fft3Δ* mutants over five days ($n = 10$, for all groups). **(D)** Box and whisker plot describing average colony size (arbitrary units) in wild-type, *tsc2-R1296P*, *fft3Δ*, and *tsc2-R1296P fft3Δ* mutants at day 5. **(E)** *tsc2-R1296P ypa1Δ* and *tsc2Δypa1Δ* double mutants suffer from similar growth perturbations. **(F)** *tsc2-R1296P fft3Δ* and *tsc2Δfft3Δ* double mutants exhibit similar growth impediment. Lower case letters represent significant differences (if any) among the groups.

A

B

C
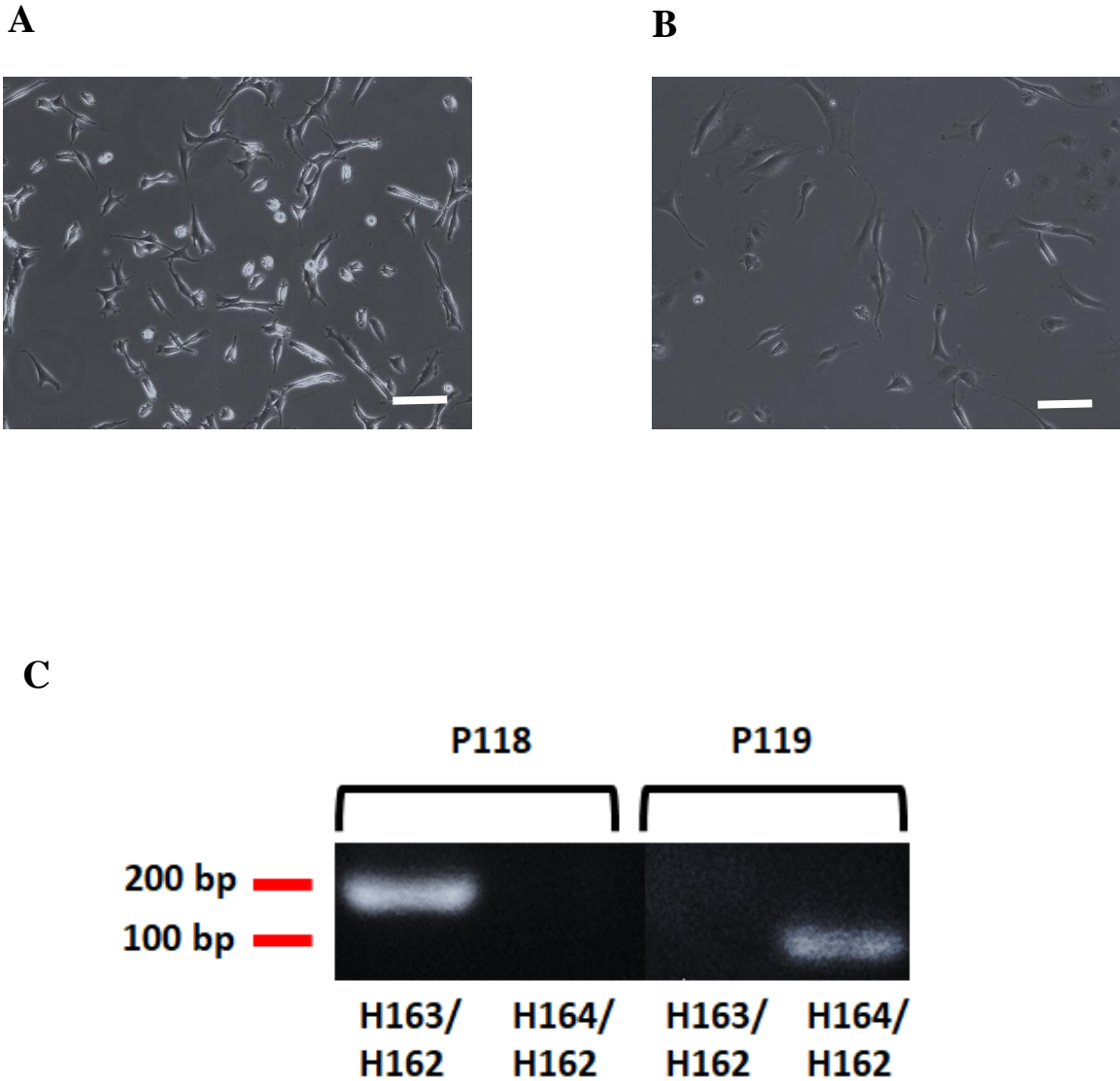
Figure 3-14: Genotyping of the P118 and P119 MEF cell lines. (**A**) Microscopic view of the P118 MEFs at passage 2, objective 20X, scale bar – 100 µm (light microscopy). (**B**) Microscopic view of the P119 MEFs at passage 3, objective 20X, scale bar – 100 µm (light microscopy). (**C**) The indicated primers (combination of H162, H163, and H164) were used to PCR amplify genomic DNA from P118 and P119 cells. The resulting amplicons were run on a 1.7% agarose gel to confirm the presence/absence of the neomycin cassette.

from H163/H162 (Figure 3-14 C). The data confirmed that exon 3 of the *Tsc2* gene is disrupted in the P119 cells, and thus induced a loss of function mutation. Hence, the P119 MEFs provided a powerful tool for examining the synthetic interactions (identified in fission yeast) in more developmentally complex eukaryotes.

3.6 Conservation of negative interactions in mouse embryonic fibroblasts

The validated interactors from the initial screen in *S. pombe* have clear orthologs in developmentally complex eukaryotes, including mice and humans. Thus, *Ppp2r4* (ortholog of *ypa1*) and *Smarcad1* (ortholog of *fft3*) were tested to see if the negative interactions were conserved in the MEFs. Both P118 and P119 cells were transfected for 48 hours with 10 µM siRNAs. Treatments with scrambled siRNA had no effects on the mRNA expressions of *Smarcad1* and *Ppp2r4* compared to the untreated samples. However, siRNAs specifically targeting the mRNA of *Smarcad1* or *Ppp2r4* greatly abolished their respective gene expressions (Figure 3-15).

Upon validation of siRNA-mediated knockdowns, cell viability was assayed to determine synthetic interactions between *Tsc2* and *Ppp2r4* or *Smarcad1*. CellTiter-Glo assays were utilized to monitor the number of viable cells based on the presence of ATP. The reagent from the assay generated stable luminescent signals which were read through a luminometer to approximate cell viability. The wild-type P118 and *Tsc2*-deficient P119 cells were transfected with either *Ppp2r4* or *Smarcad1* siRNAs. Results showed that both *Ppp2r4* and *Smarcad1* siRNA treatments had no effects on cell viability of the P118 MEFs ($p > 0.05$ for all pairwise comparisons with control group; Figure 3-16 A). Interestingly, the *Ppp2r4* siRNA-mediated knockdown in the *Tsc2*-deficient P119 MEFs demonstrated a

significant reduction in the cell viability (~ 26% reduction, $p = 0.01$ for the pairwise comparison with control group; Figure 3-16 B). This supports the hypothesis that negative interaction between *tsc2* and *ypa1* witnessed in fission yeast may indeed be conserved in mammals. *Smarcad1*, however, did not show a similar trend of negative interaction with *Tsc2* ($p = 0.22$ for pairwise comparison with control group; Figure 3-16 B).
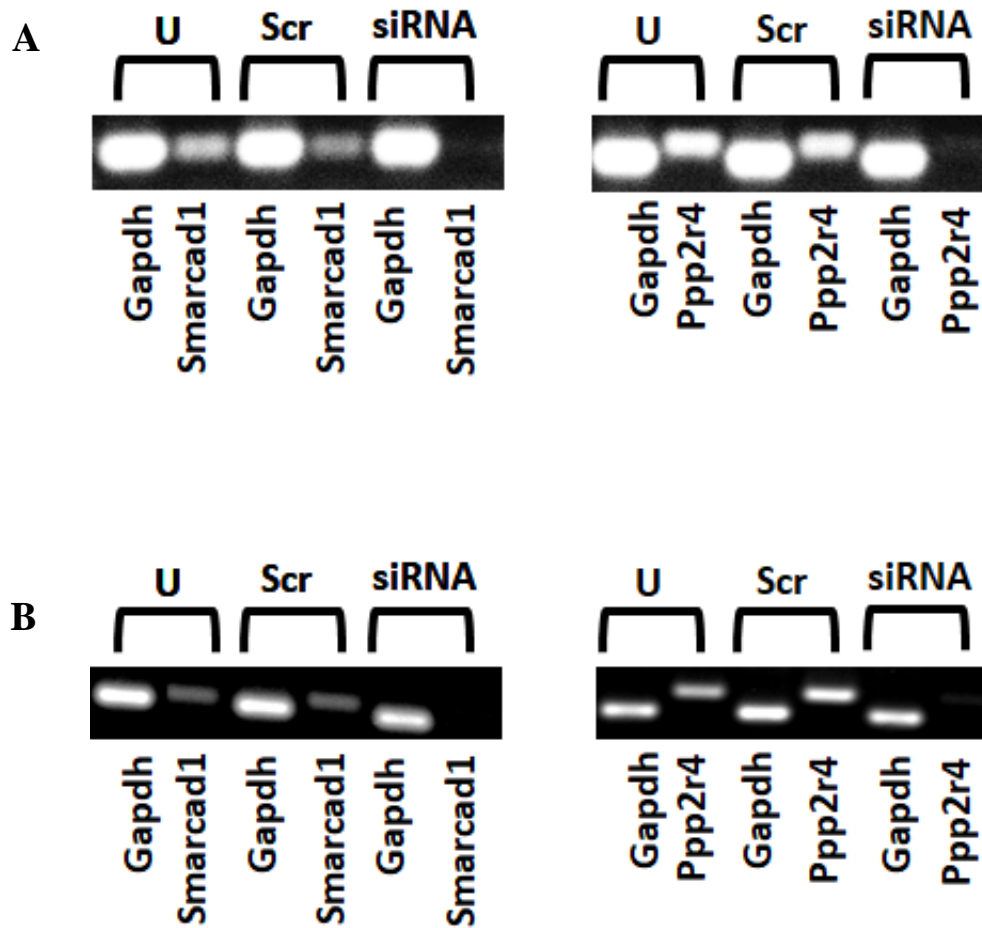
Figure 3-15: siRNA knockdown at 48 hours. (**A**) *Smarcad1* and *Ppp2r4* gene expression in P118 cells is abolished upon siRNA treatments (lane 6 of each image). (**B**) *Smarcad1* and *Ppp2r4* gene expression in P119 cells is abolished upon siRNA treatments (lane 6 of each image). The housekeeping gene, *Gapdh* was used as a control. U = untreated cells, Scr = negative control siRNA targeting no known mouse genes, siRNA = corresponding siRNA used to knockdown gene of interest.
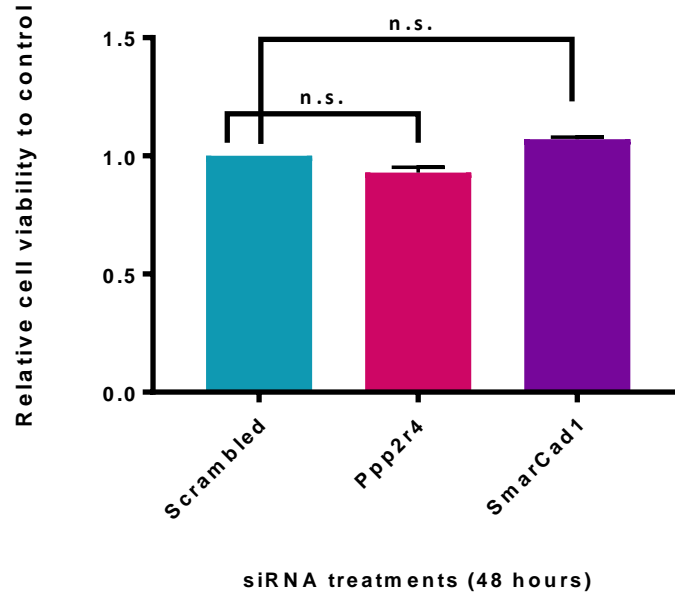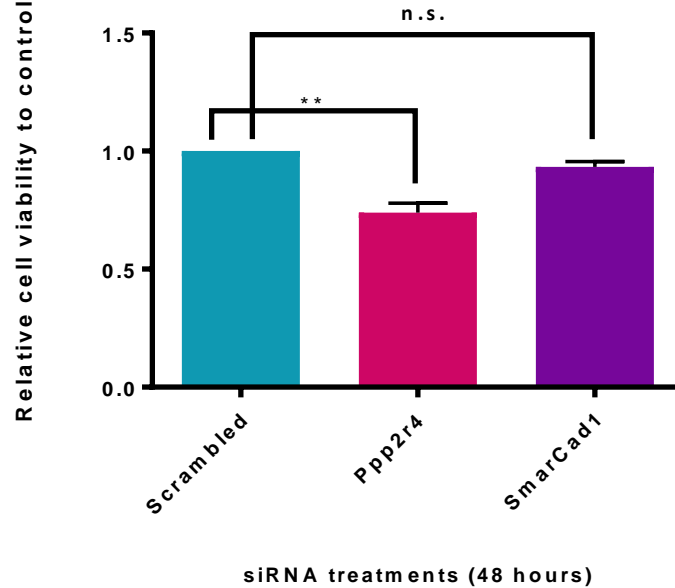
Figure 3-16: Cell viability of MEFs 48 hours following siRNA treatment. (**A**) Relative cell viability of P118 cells treated with a scrambled siRNA control or siRNAs targeting *Ppp2r4*, or *Smarcad1* ($n = 3$, for all groups). (**B**) Relative cell viability of P119 cells treated with a scrambled siRNA control or siRNAs targeting *Ppp2r4*, or *Smarcad1* ($n = 3$, for all groups). Statistical analyses were performed using the Friedman test in GraphPad Prism v7.0.2. **$p = 0.01$; n.s. denotes a statistically insignificant difference.

CHAPTER IV: DISCUSSION

The primary objective of this study was to explore the genetic interaction network underlying tuberous sclerosis complex. This was done in part to elucidate the mechanism of the TSC pathogenesis; but, also to identify prospective drug targets for novel therapeutic strategies. The study looked to utilize large-scale genetic buffering relationships discovered in fission yeast to reveal negative interactors of both *tsc1* and *tsc2*. In addition, RNAi knockdowns in mammalian cells were used to further assess any promising candidates screened through the fission yeast genetic interactions.

4.1 Overview of the fission yeast genetic interactome

Genetic interactions are vital in the translation of genotypic information to phenotypic consequences. These networks are known to be important in understanding complex human diseases and may play a role in the mystery of 'missing heritability' (Horn et al., 2011; Zuk et al., 2012). Analyses in model systems support the notion that genetic interactions between alleles can inflate variation and phenotypic outcomes (Horn et al., 2011). Unlike protein-protein interactions, genetic interactions are not limited to physical association between their respective encoded proteins (Ryan et al., 2012). In fact, only ~1% of the genetic interactions overlap with corresponding protein-protein interactions (Boone et al., 2007; Tong et al., 2004). Instead, genetic interactomes provide invaluable information with respect to functional attributes of genes and often reveal the role of gene products involved in functionally related pathways (Boone et al., 2007; Ryan et al., 2012). Most genes exhibit few genetic interactions, while a few genes ('hubs') are highly

connected in the interaction map and are more likely to be functionally important (Tong et al., 2004).

The budding yeast *S. cerevisiae* was first analyzed to generate large-scale genetic interaction networks (Costanzo et al., 2010). However, such analysis in the distantly related *S. pombe* was limited to small scale investigations of specific pathways and cellular processes (Roguev et al., 2007; Roguev et al., 2008). Nonetheless, a quantitative and genome-wide *S. pombe* genetic interactome was recently mapped, encompassing ~50% of the genome with ~1.6 million generated digenic interactions (Ryan et al., 2012). In addition, the group annotated numerous functions to previously uncharacterized genes. The generation of this powerful dataset provided an opportunity to examine prospective synthetic interactions concerning tuberous sclerosis complex.

4.2 Characterization of the validated negative interactors

Fission yeast Tsc1p and Tsc2p act in pathways akin to their respective homologs in humans (TSC1 and TSC2). This study aimed to exploit recent work (Housden et al., 2015; Ryan et al., 2012) to identify negative interactor genes of both *tsc1* and *tsc2* in fission yeast. The colony growth assays validated *ypa1* and *fft3*, but not *cdk11*, as negative interactors of *tsc1* and *tsc2* (Figure 3-2 to 3-4). The data were in accordance with the prediction that complete gene deletions of *ypa1* and *fft3* in *tsc1Δ* and *tsc2Δ* backgrounds would result in severe reduction of colony growth size.

Fission yeast *ypa1* encodes the protein – phosphotyrosyl phosphatase activator (PTPA, also known as Ypa1p). Little is known about fission yeast PTPA, except that it regulates the activity of serine/threonine protein phosphatase 2A (PP2A) (Goyal and

Simanis, 2012). Likewise, the budding yeast PTPA (encoded by *rrd1*) regulate the catalytic activity of PP2A, which is a known associate of the TOR pathway (Poschmann et al., 2011; Van Hoof et al., 2000; Zheng and Jiang, 2005). Mutants bearing *rrd1Δ* have several morphological defects including irregular progression through G1/S transition of the cell cycle (Jordens et al., 2006; Van Hoof et al., 2001). Interestingly, researchers have discovered that DNA-dependent protein kinase (DNA-PK) activation by PP2A is required for the repair of double stranded breaks (DSBs) through non-homologous end joining (NHEJ) (Li et al., 2013) and the process is known to occur primarily in the G1 phase (Chen et al., 2011). Additionally, PTPA association with RNA polymerase II (RNAPII) is crucial in the regulation of stress-responsive genes (Poschmann et al., 2011). In *rrd1Δ* mutants, transcriptional control may be lost due to RNAPII disassociation from the coding sequences (Sen et al., 2014). Taken together, budding yeast PTPA may act to regulate the TOR pathways and the NHEJ pathway of DNA repair indirectly through PP2A activity, and work directly to activate RNAPII mediated transcription of stress-responsive genes. Whether the *S. pombe* PTPA participates in DNA damage repair and the regulation of the cell cycle in similar ways requires more comprehensive analyses.

The Fft3 protein is a Swi/Snf2 family ATP-dependent chromatin remodeler that is greatly conserved across many eukaryotes (Steglich et al., 2015). Previous work has demonstrated that Fft3p is essential in maintaining the heterochromatin structure of the centromeric and sub-telomeric regions and plays a role in the regulation of the overall nuclear organization (Steglich et al., 2015; Strålfors et al., 2011). In *S. pombe*, *fft3Δ* results in euchromatin formation leading to incorrect histone modifications and mis-regulation of gene expression (Strålfors et al., 2011). Thus, Fft3p may be crucial in key cellular processes

such as transcription, DNA repair and DNA replication (Steglich et al., 2015). Interestingly, Fft3p orthologs – Fun30 in *S. cerevisiae* and SMARCAD1 in humans, are known to aid in DNA end resection of DSBs via G2 cell cycle homologous recombination (HR) (Chen et al., 2012; Costelloe et al., 2012; Eapen et al., 2012). Inability to successfully repair DSBs compromises genome integrity and leads to prolonged G1/G2 checkpoint arrest which often results in apoptosis (Massagué, 2004). Fun30 can increase the rate of the 5'-to-3' DNA resection and deactivate the G2/M DNA damage checkpoint arrest (Eapen et al., 2012). This is done at the chromatin level, where Fun30 (as well as the human homolog SMARCAD1) can relax the tight histone-DNA interactions in nucleosomes adjacent to DSBs (Chen et al., 2012; Costelloe et al., 2012). In fission yeast, however, the precise mechanism of the Fft3p role in the DNA damage repair has not been explored.

As discussed earlier, genetic interactions rarely implicate physically associated gene products (Tong et al., 2004). Furthermore, only a small subset of strong negative interactions amount to interactions in 'within-pathway' complexes (Costanzo et al., 2011). In *S. cerevisiae*, most synthetic lethal interactions, albeit rare, occur between genes with similar cellular functions (Tong et al., 2004). Fission yeast hamartin-tuberin heterodimeric complex have been shown to play a role in the regulation of nutrient uptake, cellular growth and stress response (Aspuria et al., 2007; Mak and Yeung, 2004); and the role of Ypa1p, Fft3p and their homologs has been discussed above. Thus, it is highly likely that the strong negative genetic interactions exhibited among *ypa1*, *fft3*, and *tsc1/2* do not correspond to physical protein-protein interactions. Instead, the results in this study suggest that the genes participate in 'between-pathway' genetic interactions. These interactions often occur

among functionally related genes in complementary biological pathways (Boone et al., 2017).

In *S. pombe*, the role of Ypa1p and Fft3p suggests that cellular processes such as transcription and DNA repair may contribute to the Tsc1p-Tsc2p controlled TOR pathways which regulates cellular growth, proliferation and stress-response. Interestingly, Ypa1p is known to regulate the activity of PP2A (Goyal and Simanis, 2012) and its budding yeast ortholog is associated with the TOR pathways (Poschmann et al., 2011; Van Hoof et al., 2000; Zheng and Jiang, 2005). Thus, the fission yeast PTPA (Ypa1p) may yet be implicated in the TOR pathways and the functional complementarity among the protein products of the genes (*ypa1*, *fft3*, *tsc1*, and *tsc2*) could provide an explanation for the strong negative interactions validated in this study.

Interestingly, however, *ypa1* and *fft3* did not demonstrate any synthetic interactions between the genes (data not shown). This finding supports the notion that Ypa1p and Fft3p are involved in different pathways that can impinge on shared function affecting cellular growth. Hence, although negative genetic interactions are frequent between genes within the same cellular pathway or pathways that are closely linked (Baryshnikova et al., 2010), it may not be a requirement. In fact, 'hub' genes can interact with numerous genes making them essential to a wide range of cellular processes (Boone et al., 2007). Therefore, these genes are crucial in modulating phenotypic variation and complexity. Whether *tsc1* and *tsc2* can be considered as 'hub' genes remain to be determined. Here, the findings suggest that the fission yeast cells with tumor-like molecular context (loss of functional *tsc1* and *tsc2*) can be selectively targeted to inhibit growth.

Hence, Ypa1p and Fft3p provide promising candidates for further investigation and are prospective drug targets in TSC therapeutics.

4.3 Applying the concept of synthetic chemical-genetic interactions

A traditional strategy for anticancer drug discovery is to assay inhibitory compounds for their ability to selectively target cells that mimic the molecular alterations of tumor cells (Hartwell et al., 1997). Using the digenic negative interaction dataset, specific pharmacological inhibitors can be screened for lethality emulating novel drug-gene synthetic interactions (Beijersbergen et al., 2017; Boone et al., 2007; Kaelin, 2005; Nijman, 2011). Inhibition of the catalytic domains in Ypa1p and Fft3p by chemical treatments in combination with *tsc1* or *tsc2* loss of function mutations, therefore, should result in cellular growth defects. In principle, this may allow for selective targeting of tumor cells (lacking functional *TSC1* and *TSC2*) using synthetic lethal chemical-genetic interactions (Boone et al., 2007). Thus, it was important to identify sites that may be amenable to chemical inhibition within the fission yeast Ypa1p and Fft3p.

The study first examined the highly conserved PPIase domain of the Ypa1p (PTPA). The PTPA PPIase domain is well conserved across eukaryotes including the budding yeast (Chao et al., 2006, Jordens et al., 2006; Leulliot et al., 2006). Proteomic analyses have shown that PTPA mutations in budding yeast aspartate[213] and valine[209] sites within the catalytic core compromised binding with PP2A (Chao et al., 2006; Leulliot et al., 2006). Also, mutations in these sites resulted in the loss of the PTPA phosphatase activity and abolished ATP-dependent activation of PP2A (Guo et al., 2014). Their orthologous *S. pombe* strains – *ypa1-D212G* and *ypa-V208D*, however, did not seem to suffer from a similar loss of function, as the double mutants with *tsc1Δ* and *tsc2Δ* did not

exhibit expected growth perturbations (Figures 3-8 and 3-9). These results suggest one of two possibilities. First, that unlike mutations in the *S. cerevisiae* PTPA, these subtle missense mutations do not cause significant conformational changes in the fission yeast PTPA and abolish the PPIase activity, or second, that the observed synthetic growth defect results from the loss-of-function of a PPIase independent activity. Interestingly, *S. cerevisiae* mutants bearing complete deletion of the catalytic PPIase domain have been shown to drastically impair the activation of PP2A (Jordens et al., 2006). The work in my study aimed to reciprocate this deletion in *S. pombe*, but was unable to generate any viable strain (data not shown).

In contrast, the ATPase dead *fft3-K418R* mutants demonstrated synthetic growth defects with both *tsc1* and *tsc2* as predicted (Figure 3-11). In fission yeast, the ATPase activity of Fft3p has been shown to maintain subtelomeric and centromeric heterochromatin structures (Steglich et al., 2015; Strålfors et al., 2011). Moreover, the ATPase domain is important to the function of many other SWI/SNF chromatin remodelers (Hargreaves and Crabtree, 2011), and is highly conserved across eukaryotes (Figure 3-7). Previous studies in *S. cerevisiae* showed that ATPase dead Fun30 mutants suffered G2 cell cycle arrest due to unsuccessful 5' to 3' DNA end resection of DSBs (Chen et al., 2012; Eapen et al., 2012). Likewise, siRNA knockdowns of SMARCAD1 (Fft3p and Fun30 homolog in humans) resulted in accumulation of cells with DNA damage and impaired DNA repair mechanisms (Costelloe et al., 2012). Furthermore, in budding yeasts, the Fun30 helicase domain is thought to be important in the remodeling of nucleosomes and efficient DNA end resection (Awad et al., 2010; Chen et al., 2012). However, the helicase-deleted fission yeast mutants (*fft3Δ791-872*) did not display synthetic growth defects with

either *tsc1* or *tsc2* (Figure 3-10). Here, the results suggest that the loss of the ATPase activity of Fft3p through a site-directed mutation (K418R) is primarily responsible for the observed negative interaction. Thus, the data suggest a prospective site of pharmacological inhibition within Fft3p that might recapitulate the negative interaction between *fft3* and *tsc1/tsc2*.

4.4 Investigation of disease-causing clinical mutations in *S. pombe*

Although mutations in *TSC1* and *TSC2* can be inherited as autosomal dominant traits (in familial cases with at least one affected parent), most cases of TSC are sporadic (~65% without an affected parent) (Narayanan, 2003). *TSC2* mutations are significantly overrepresented among sporadic cases of the disease (Jones et al., 1999; Napolioni and Curatolo, 2008). Furthermore, clinical phenotypes arising from patients with *TSC2* mutations are more severe (Franz and Weiss, 2012; Mak and Yeung, 2004; Neuman and Henske, 2011). Thus, the study sought to investigate clinical *TSC2* mutations. Six *S. pombe* strains with *tsc2* alleles bearing orthologous *TSC2* missense mutations were examined, to test for synthetic interactions with the validated negative interactors – *ypa1* and *fft3* (Figure 3-12). The data indicated that only the *tsc2-R1296P* allele exhibits synthetic growth defects with both *ypa1Δ* and *fft3Δ*, as previously predicted (Figure 3-13).

The tuberin GAP domain is well conserved in *S. pombe* with ~ 45% amino acid sequence similarity (Neuman and Henske, 2011; Serfontein et al., 2011). Three disease-causing missense mutations within this domain are frequent within TSC patients – N1643K, N1651S, and P1675L (Jones et al., 1999). Their corresponding orthologous mutations in *S. pombe* (N1191K, N1199S, and P1223L) have been shown to limit nutrient

uptake and arginine biosynthesis underlining a unique function of the fission yeast Tsc2p GAP domain (van Slegtenhorst et al., 2004). Here, the absence of negative genetic interactions involving these mutants in *ypa1Δ* and *fft3Δ* backgrounds suggest that these mutations do not cause synthetic growth defects that were witnessed when *tsc2* was fully deleted. Likewise, two other mutant strains outside the Tsc2p GAP domain (G296E and R927W) were tested and exhibited normal colony growth. The results, therefore, indicate that either these missense mutations in fission yeast do not attribute to loss of Tsc2p functions contrary to their orthologous mutations in clinical TSC cases or, that the negative interactions between *tsc2* and *ypa1* or *fft3* is conditional on loss of tuberin completely.

The arginine^{1743} and arginine^{1745} sites exist outside the GAP domain near the C-terminus of TSC2 (Jones et al., 1999). Surprisingly, mutations in these sites (R1743P and R1745Q) abolish the GAP activity of TSC2 and result in the inability to phosphorylate downstream p70S6K1 (Li et al., 2004). Patients bearing these mutations therefore suffer from the TSC pathology due to an indirect mis-regulation of the tuberin GAP activity (Li et al., 2004). In fission yeast, the patient-derived arginine sites are conserved as R1296 and R1298 sites. Although, the orthologous *tsc2-R1298Q* strain was not included in this study, the synthetic growth defects exhibited by *S. pombe* strains bearing the *tsc2-R1296P* allele indicate that this specific site may indeed be important for functional Tsc2p activity. Thus, negative interactions between clinically orthologous mutations, and *ypa1* or *fft3* do not appear to be conditional on the complete loss of tuberin. Additionally, the synthetic genetic interactions between *tsc2-R1296P* allele with both *ypa1* and *fft3* may allude to a broader conservation of these negative interactions across TSC patients and warrants a more comprehensive analysis of the diverse *TSC1* and *TSC2* mutations.

4.5 Conservation of synthetic interactions

Previous work has focused on the conservation of genetic interactions across the distantly related eukaryotes, *S. pombe* and *S. cerevisiae* (Dixon et al., 2008; Roguev et al., 2008). The two unicellular yeasts share 30% of the genetic interactome (Dixon et al., 2008; Roguev et al., 2008). Given the ~ 400 million years of evolutionary separation between the species, this rate of conservation is extensive. Moreover, a large-scale RNAi screen in the nematode *Caenorhabditis elegans* identified a set of 'hub' genes that share numerous genetic interactions (Lehner et al., 2006). These genes encode highly conserved chromatin regulators and their genetic interactions are conserved across species (Lehner et al., 2006). Genetic interactions between genes within the same pathway tend to be conserved at a higher rate (~ 45%) than those belonging to different processes (~15%) (Ryan et al., 2012). The negative interactions examined in this study (among *ypa1*, *fft3*, *tsc1,* and *tsc2*) are presumably involved in 'between-pathway' genetic interactions; and such interactions are less frequently conserved, at a rate of ~ 15% (compared to the ~35% conservation rate for 'within-pathway' negative interactions) (Ryan et al., 2012).

Nonetheless, a recent breakthrough using CRISPR-based *Tsc2*-knockout *Drosophila spp.* cell lines and *Tsc2*$^{-/-}$ MEFs demonstrated that TSC-specific synthetic interactions may indeed be conserved in higher eukaryotes (Housden et al., 2015). Further assessment of these interactions in these *Tsc2*-deficient MEFs was essential to evaluating prospective drug targets identified in this study. siRNA knockdowns of the *ypa1* and *fft3* homologs – *Ppp2r4* and *Smarcad1*, in the *Tsc2*-deficient mammalian cells abolished their respective gene expression (Figure 3-15). However, only the *Ppp2r4* knockdown resulted in decreased cellular viability in *Tsc2*$^{-/-}$ MEFs compared to the wild type cells (Figure 3-

16). In contrast, the *Smarcad1* knockdown had no effects on the survivability of the *Tsc2*-deficient MEFs. Altogether, this study provide evidence that, while some genetic buffering relationships may be conserved across species, others are not. This phenomenon may be explained by the possibility of functional 'repurposing' as a result of evolutionary divergence and associations of genetic interactions, in addition to the widespread conservation among species (Frost et al., 2012). Nonetheless, the results here suggest that the *Ppp2r4* gene product in humans, PPP2R4, might represent an ideal drug target and, thus, may contribute to novel therapeutic strategies to combat the TSC pathology.

4.6 Implications, challenges and future directions

The understanding of human biology and diseases goes beyond the functions of single genes in isolation (Hartman IV et al., 2001). Complex genetic interaction networks are involved in a multitude of phenotypic consequences including genetic disorders and disease. Genome-wide studies of genetic interactions have led to construction of large-scale interactomes that provide an opportunity to visualize such complexity (Boone et al., 2007). In particular, synthetic relationships have played a vital role in the understanding of disease mechanisms, drug discovery and novel therapeutic strategies (Nijman, 2011). This study sought to utilize the recently developed *S. pombe* genetic interactome to elucidate the molecular pathology of tuberous sclerosis complex and to identify novel disease-specific drug targets.

Although the efforts of this study have led to the discovery of a prospective TSC-specific drug target PPP2R4, limitations remain. First, the isogenic *S. pombe* strains and MEFs used in this study present an inevitable quandary. They are invaluable tools in

evaluating the fitness of single mutants with those of the double mutants and help elucidate gene buffering relationships (Hartman IV et al., 2001). However, the isogenic background of these strains and cell lines often ignores background differences and simplifies the complexity within these model systems and thus, limit understanding at a deeper level. Also, RNAi tools used in this study offer incomplete transfection, partial gene knockdowns, and can have frequent off-target effects leading to false negatives and positives (Housden et al., 2015). Therefore, the conservation of the synthetic interactions across species requires a more complete examination. Additionally, this study solely focused on these interactions in cells mimicking loss-of-function mutations in *TSC2* (*Tsc2*$^{-/-}$ MEFs). Thus, a comprehensive analysis should look to include investigation in cellular contexts bearing *TSC1* loss-of-function mutations. Interestingly, Housden et al. (2015) developed *TSC1* and *TSC2* mutant lines in *Drosophila spp.* and thus, present an opportunity for in-depth examination in a different model system.

Second, the characterization of the negative interactors was limited in the context of this work. Fission yeast *ypa1* is poorly understood (Goyal and Simanis, 2012) and thus, requires extensive cellular and molecular analysis to determine the exact role of the PTPA gene product (also known as Ypa1p). In contrast, *fft3* is relatively well studied in *S. pombe*, with roles in heterochromatin preservation, transcription, epigenetic inheritance and DNA replication (Steglich et al., 2015; Strålfors et al., 2011; Taneja et al., 2017); however, the detailed machineries of the Fft3p is yet to be explored. Altogether, a comprehensive study of these interactors and their orthologs in humans may help generate useful insights into the mechanisms of their corresponding gene products, and such information combined with

the genetic interaction data may help provide a greater understanding of the tuberous sclerosis pathogenesis.

Third, a widespread phenomenon known as NGE can drastically affect large-scale genetic interaction data sets (Ben-Shitrit et al., 2012). NGEs can arise from the effects of gene deletions on the expression of adjacent genes along the genome (Atias et al., 2015). While the mechanism of these effects remains unknown, it is possible that the deletion of a given locus alters chromatin structure and/or the regulatory characteristics of adjacent loci (Baryshnikova and Andrews, 2012). Recent analysis of the *S. cerevisiae* genetic interactome has revealed that ~ 10% of the scored genetic interactions are affected by NGE and the corresponding data sets may be erroneous (Atias et al., 2015). Efforts were made to investigate NGE effects on the synthetic interactions observed in this study (Figures 3-5 and 3-6). Although the data strongly suggest absence of any NGE effects, the analysis is not nearly comprehensive enough. Only two adjacent gene deletions were tested for NGE effects on each negative interactor (*ypa1* and *fft3*). Thus, the need to increase the number of genes included in the NGE studies is apparent. Future annotations of genetic interactions may look to utilize recently developed algorithms (Atias et al., 2015; Ben-Shitrit et al., 2012), that are capable of not only detecting these interactions, but also finding ways to correct them.

Lastly, although the *S. pombe* genetic interaction data sets are considered large-scale and encompasses ~ 50% of the genome, it is not entirely complete and suffers from limitations. In fact, the more established *S. cerevisiae* genetic interactome corresponds to only ~ 2% of all genetic interactions within a typical mammalian cells (Ryan et al., 2012). Thus, the translation of genetic interaction studies from unicellular eukaryotes such as

fission yeast to higher eukaryotes presents difficulty. The presence of multiple tissues, numerous cell types and intricate signaling networks in higher eukaryotes can further add to the complexity. This obscures the evaluation of any prospective candidates for TSC-specific therapeutic intervention identified through the fission yeast genetic interactome. More complete and diverse analyses are thus required in multiple TSC disease-models in addition to the *Tsc2^{-/-}* MEFs used in this study. Interestingly, patient derived *TSC2*-deficient lymphangioleiomyomatosis (LAM) cells have proven a useful model in studying tumorigenesis (Li et al., 2014). Furthermore, recent advances in platforms such as shRNA knockdown and CRISPR/Cas9-mediated gene knockouts have also made it possible to perform synthetic screens for numerous pairs of genes in a large population of cells (Beijersbergen et al., 2016). Thus, future studies should aim to utilize these technological advances to generate a more comprehensive mammalian genetic interactome from various tissues and cell types.

In conclusion, by combining the genome-wide fission yeast interactome with TSC-specific genetic networks, this study has helped to shed insights into the molecular pathology of tuberous sclerosis complex. In TSC patients, loss of a functional TSC1-TSC2 heterodimer causes over activation of mTORC1, resulting in increased metabolic and oxidative cellular stresses (Beijersbergen et al., 2016). In tumor cells, the rate of cellular metabolism increases greatly as the requirement of various cellular processes is enhanced (Kroemer and Pouyssegur 2008). Inhibiting key components in the metabolic processes can severely impair tumor cells while leaving normal cells relatively unaffected, as the tumor-specific cells become highly prone to growth arrest and subsequent cell death (Kroemer and Pouyssegur 2008). Hence, targeted inhibition of PPP2R4 might represent an

"Achilles' heel" of the TSC-specific tumors and represents a novel drug target for therapeutic intervention. The robustness of this investigation is demonstrated by the discovery of a disease-specific drug target utilizing genetic interaction biology (Beijersbergen et al., 2016), suggesting that such data sets are invaluable in understanding complex human disorders and may aid in future disease-associated inquiries.

LITERATURE CITED

Abràmoff, M.D., Magalhães, P.J., and Ram, S.J. (2004). Image processing with ImageJ. Biophotonics International *11*, 36-41.

Aspuria, P.-J., Sato, T., and Tamanoi, F. (2007). The TSC/Rheb/TOR signaling pathway in fission yeast and mammalian cells: Temperature sensitive and constitutive active mutants of TOR. Cell Cycle *6*, 1692-1695.

Astrinidis, A., and Henske, E.P. (2005). Tuberous sclerosis complex: linking growth and energy signaling pathways with human disease. Oncogene *24*, 7475-7481.

Atias, N., Kupiec, M., and Sharan, R. (2015). Systematic identification and correction of annotation errors in the genetic interaction map of *Saccharomyces cerevisiae*. Nucleic Acids Research *44*, e50.

Awad, S., Ryan, D., Prochasson, P., Owen-Hughes, T., and Hassan, A.H. (2010). The Snf2 homolog Fun30 acts as homodimeric ATP-dependent chromatin-remodeling enzyme. Journal of Biological Chemistry *285*, 9477-9484.

Baryshnikova, A., and Andrews, B. (2012). Neighbouring-gene effect: a genetic uncertainty principle. Nature Methods *9*, 341-343.

Baryshnikova, A., Costanzo, M., Kim, Y., Ding, H., Koh, J.L.Y., Toufighi, K., Youn, J.-Y., Ou, J., San Luis, B.-J., Bandyopadhyay, S., et al. (2010). Quantitative analysis of fitness and genetic interactions in yeast on a genome scale. Nature Methods *7*, 1017-1024.

Baryshnikova, A., Costanzo, M., Myers, C.L., Andrews, B., and Boone, C. (2013). Genetic interaction networks: toward an understanding of heritability. Annual Review of Genomics and Human Genetics *14*, 111-133.

Beijersbergen, R.L., Wessels, L.F.A., and Bernards, R. (2017). Synthetic lethality in cancer therapeutics. Annual Review of Cancer Biology *1*, 1-21.

Benjamin, D., and Hall, M.N. (2014). mTORC1: Turning off is just as important as turning on. Cell *156*, 627-628.

Ben-Shitrit, T., Yosef, N., Shemesh, K., Sharan, R., Ruppin, E., and Kupiec, M. (2012). Systematic identification of gene annotation errors in the widely used yeast mutation collections. Nature Methods *9*, 373-378.

Boones, C., Bussey, H., and Andrews, B.J. (2007). Exploring genetic interactions and networks with yeast. Nature Reviews Genetics *8*, 437-449.

Byeon, B., Wang, W., Barski, A., Ranallo, R.T., Bao, K., Schones, D.E., Zhao, K., Wu, C., and Wu, W.-H. (2013). The ATP-dependent chromatin remodeling enzyme Fun30 represses transcription by sliding promoter-proximal nucleosomes. Journal of Biological Chemistry *288*, 23182–93.

Chao, Y., Xing, Y., Chen, Y., Xu, Y., Lin, Z., Li, Z., Jeffrey, P.D., Stock, J.B., and Shi, Y. (2006). Structure and mechanism of the phosphotyrosyl phosphatase activator. Molecular Cell *23*, 535-546.

Chen, H., Ma, Z., Vanderwaal, R.P., Feng, Z., Gonzalez-Suarez, I., Wang, S., Zhang, J., Roti Roti, J.L., Gonzalo, S., and Zhang, J. (2011). The mTOR inhibitor rapamycin suppresses DNA double-strand break repair. Radiation Research *175*, 214-224.

Chen, X., Cui, D., Papusha, A., Zhang, X., Chu, C.-D., Tang, J., Chen, K., Pan, X., and Ira, G. (2012). The Fun30 nucleosome remodeller promotes resection of DNA double-strand break ends. Nature *489*, 576–580.

Collins, S.R., Miller, K.M., Maas, N.L., Roguev, A., Fillingham, J., Chu, C.S., Schuldiner, M., Gebbia, M., Recht, J., Shales, M., et al. (2007). Functional dissection of protein complexes involved in yeast chromosome biology using a genetic interaction map. Nature *446*, 806-810.

Costa-Cabral, S., Brough, R., Konde, A., Aarts, M., Campbell, J., Marinari, E., Riffell, J., Bardelli, A., Torrance, C., Lord, C.J., et al. (2016). CDK1 is a synthetic lethal target for KRAS mutant tumours. PLoS One *11*, e0149099.

Costanzo, M., Baryshnikova, A., Bellay, J., Kim, Y., Speard, E.D., Sevier, C.S., Ding, H., Koh, J.L.Y., Tougfighi, K., Mostafavi, S., et al. (2010). The genetic landscape of a cell. Science *327*, 425-431.

Costanzo, M., Baryshnikova, A., Myers, C.L., Andrews, B., and Boone, C. (2011). Charting the genetic interaction map of a cell. Current Opinion in Biotechnology *22*, 66–74.

Costelloe, T., Louge, R., Tomimatsu, N., Mukherjee, B., Martini, E., Khadaroo, B., Dubois, K., Wiegant, W.W., Thierry, A., Burma, S., et al. (2012). The yeast Fun30 and human SMARCAD1 chromatin remodellers promote DNA end resection. Nature *489*, 581–584.

Dalle Pezze, P., Sonntag, A.G., Thien, A., Prentzell, M.T., Gödel, M., Fischer, S., Neumann-Haefelin, E., Huber, T.B., Baumeister, R., Shanley, D.P., et al. (2012). A dynamic network model of mTOR signaling reveals TSC-independent mTORC2 regulation. Science Signaling *5*, ra25.

De Virgilio, C., and Loewith, R. (2006). Cell growth control: little eukaryotes make big contributions. Oncogene *25*, 6392-6415.

Dixon, S.J., Fedyshyn, Y., Koh, J.L.Y., Keshava Prasad, T.S., Chahwan, C., Chua, G., Toufighi, K., Baryshnikova, A., Hayles, J., and Hoe, K.-L., et al. (2008). Significant conservation of synthetic lethal genetic interaction networks between distantly related eukaryotes. Proceedings of the National Academy of Sciences of USA *105*, 16653–16658.

Durand-Dubief, M., Will, W.R., Petrini, E., Theodorou, D., Harris, R.R., Crawford, M.R., Paszkiewicz, K., Krueger, F., Correra, R.M., Vetter, A.T., et al. (2012). SWI/SNF-like chromatin remodeling factor Fun30 supports point centromere function in *S. cerevisiae*. PLoS Genetics *8*, e1002974.

Eapen, V.V., Sugawara, N., Tsabar, M., Wu, W.-H., and Haber, J.E. (2012). The *Saccharomyces cerevisiae* chromatin remodeler Fun30 regulates DNA end

resection and checkpoint deactivation. Molecular and Cellular Biology *32*, 4727–4740.

Forsburg, S.L. (2005). The yeasts *Saccharomyces cerevisiae* and *Schizosaccharomyces pombe*: models for cell biology research. Gravitational and Space Biology *18*, 3-9.

Forsburg, S.L., and Rhind, N. (2006). Basic methods for fission yeast. Yeast *23*, 173-183.

Franz, D.N., and Weiss, B.D. (2012). Molecular therapies for tuberous sclerosis and neurofibromatosis. Current Neurology and Neuroscience Reports *12*, 294–301.

Frost, A., Elgort, M.G., Brandman, O., Ives, C., Collins, S.R., Miller-Vedam, L., Weibezahn, J., Hein, M.Y., Poser, I., Mann, M., et al. (2012). Functional repurposing revealed by comparing *S. pombe* and *S. cerevisiae* genetic interactions. Cell *149*, 1339-1352.

Gietz, D., St. Jean, A., Woods, R.A., and Schiestl, R.H. (1992). Improved method for high efficiency transformation of intact yeast cells. Nucleic Acids Research *20*, 1425.

Gonzalez, S., and Rallis, C. (2017). The TOR signaling pathway in spatial and temporal control of cell size and growth. Frontiers in Cell and Developmental Biology *5*, 1-6.

Goyal, A., and Simanis, V. (2012). Characterization of *ypa1* and *ypa2*, the *Schizosaccharomyces pombe* orthologs of the peptidyl proyl isomerases that activate PP2A, reveals a role for Ypa2p in the regulation of cytokinesis. Genetics *190*, 1235–1250.

Guo, F., Stanevich, V., Wlodarchak, N., Sengupta, R., Jiang, L., Satyshur, K.A., and Xing, Y. (2014). Structural basis of PP2A activation by PTPA, an ATP-dependent activation chaperone. Cell Research *24*, 190-203.

Hargreaves, D.C., and Crabtree, G.R. (2011). ATP-dependent chromatin remodeling: Genetics, genomics and mechanisms. Cell Research *21*, 396-420.

Hartman IV, J.L., Garvik, B., and Hartwell, L. (2001). Principles for the buffering of genetic variation. Science *291*, 1001–1005.

Hartwell, L.H., Szankasi, P., Roberts, C.J., Murray, A.W., and Friend, S.H. (1997). Integrating genetic approaches into the discovery of anticancer drugs. Science *278*, 1064-1068.

Hengstschläger, M., Rodman, D.M., Miloloza, A., Ottnad-Hengstschläger, E., Rosner, M., and Kubista, M. (2001). Tuberous sclerosis gene products in proliferation control. Mutation Research *488*, 233-239.

Hoffman, C.S., Wood, V., and Fantes, P.A. (2015). An ancient yeast for young geneticists: A primer on the *Schizosaccharomyces pombe* model system. Genetics *201*, 403-423.

Horn, T., Sandmann, T., Fischer, B., Axelsson, E., Huber, W., and Boutros, M. (2011). Mapping of signaling networks through synthetic genetic interaction analysis by RNAi. Nature Methods *8*, 341-346.

Housden, B.E., Valvezan, A.J., Kelley, C., Sopko, R., Hu, Y., Roesel, C., Lin, S., Buckner, M., Tao, R., Yilmazel, B., et al. (2015). Identification of potential drug targets for tuberous sclerosis complex by synthetic screens combining CRISPR-based knockouts with RNAi. Science Signaling *8*, rs9.

Jones, A.C., Shyamsundar, M.M., Thomas, M.W., Maynard, J., Idziaszczyk, S., Tomkins, S., Sampson, J.R., and Cheadle, J.P. (1999). Comprehensive mutation analysis of TSC1 and TSC2–and phenotypic correlations in 150 families with tuberous sclerosis. Annual Journal of Human Genetics *64*, 1305-1315.

Jordens, J., Janssens, V., Longin, S., Stevens, I., Martens, E., Bultynck, G., Engelborghs, Y., Lescrinier, E., Waelneks, E., Goris, J., et al. (2006). The protein phosphatase 2A phosphatase activator is a novel peptidyl-prolyl cis/trans-isomerase. Journal of Biological Chemistry *281*, 6349–6357.

Jouvet, N., Poschmann, J., Douville, J., Marrakchi, R., and Ramotar, D. (2011). RNA polymerase II degradation in response to rapamycin is not mediated through ubiquitylation. Biochemical and Biomedical Research Communications *413*, 248-253.

Jozwiak, J. (2006). Hamartin and tuberin: working together for tumour suppression. International Journal of Cancer *118*, 1–5.

Jozwiak, J., Jozwiak, S., and Wlodarski, P. (2008). Possible mechanisms of disease development in tuberous sclerosis. Lancet Oncology *9*, 73–79.

Kaelin, W.G. (2005). The concept of synthetic lethality in the context of anticancer therapy. Nature Reviews Cancer *5*, 689-698.

Kenerson, H., Dundon, T.A., and Yeung, R.S. (2005). Effects of rapamycin in the eker rat model of tuberous sclerosis complex. Pediatric Research *57*, 67–75.

Kim, D.-U., Hayles, J., Kim, D., Wood, V., Park, H.-O., Won, M., Yoo, H.-S., Duhig, T., Nam, M., Palmer, G., et al. (2010). Analysis of a genome-wide set of gene deletions in the fission yeast *Schizosaccharomyces pombe*. Nature Biotechnology *28*, 617-623.

Kitami, T., and Nadeau, J.H. (2002). Biochemical networking contributes more to genetic buffering in human and mouse metabolic pathways than does gene duplication. Nature Genetics *32*, 191-194.

Kroemer, G., and Pouyssegur, J. (2008). Tumor cell metabolism: cancer's Achilles' heel. Cancer Cell *13*, 472-482.

Laplante, M., and Sabatini, D.M. (2012). mTOR signaling in growth control and disease. Cell *149*, 274–293.

Lehner, B., Crombie, C., Tischler, J., Fotunato, A., and Fraser, A.G. (2006). Systematic mapping of genetic interactions in *Caenorhabditis elegans* identifies common modifiers of diverse signaling pathways. Nature Genetics *38*, 896-903.

Leulliot, N., Vicentini, G., Jordens, J., Quevillon-Cheruel, S., Schiltz, M., Barford, D., Van Tilbeurgh, H., and Goris, J. (2006). Crystal structure of the PP2A phosphatase activator: Implications for its PP2A-specific PPIase activity. Molecular Cell *23*, 413–424.

Li, C., Lee, P.-S., Sun, Y., Gu, X., Zhang, E., Guo, Y., Wu, C.-L., Auricchio, N., Priolo, C., Li, J., et al. (2014). Estradiol and mTORC2 cooperate to enhance prostaglandin biosynthesis and tumorigenesis in TSC2-deficient LAM cells. Journal of Experimental Medicine *211*, 15-28.

Li, D., Shimamura, T., Ji, H., Chen, L., Haringsma, H.J., McNamara, K., Liang, M.-C., Perera, S.A., Zaghlul, S., Borgman, C.L., et al. (2007). Bronchial and peripheral murine lung carcinomas induced by T790M-L858R mutant EGFR respond to HKI-272 and rapamycin combination therapy. Cancer Cell *12*, 81–93.

Li, Y., Inoki, K., and Guan, K.-L. (2004). Biochemical and functional characterizations of small GTPase Rheb and TSC2 GAP activity. Molecular and Cellular Biology *24*, 7965-7975.

Li, Y., Wang, X., Yue, P., Tao, H., Ramalingam, S.S., Owonikoko, T.K., Deng, X., Wang, Y., Fu, H., et al. (2013). Protein phosphatase 2A and DNA-dependent protein kinase are involved in mediating rapamycin-induced Akt phosphorylation. Journal of Biological Chemistry *288*, 13215-13224.

Mak, B.C., and Yeung, R.S. (2004). The tuberous sclerosis complex genes in tumor development. Cancer Investigation *22*, 588–603.

Manning, B.D., and Cantley, L.C. (2003). Rheb fills a GAP between TSC and TOR. Trends in Biochemical Sciences *28*, 573–576.

Massagué, J. (2004). G1 cell-cycle control and cancer. Nature *432*, 298-306.

Matsuo, T., Otsubo, Y., Urano, J., Tamanoi, F., and Yamamoto, M. (2007). Loss of the TOR kinase Tor2 mimics nitrogen starvation and activates the sexual development pathway in fission yeast. Molecular and Cellular Biology *27*, 3154-3164.

Menon, S., Dibble, C.C., Talbott, G., Hoxhaj, G., Valvezan, A.J., Takahashi, H., Cantley, L.C., and Manning, B.D. (2014). Spatial control of the TSC complex integrates insulin and nutrient regulation of mTORC1 at the lysosome. Cell *156*, 1771–1785.

Napolioni, V., and Curatolo, P. (2008). Genetics and molecular biology of tuberous sclerosis complex. Current Genomics *9*, 475–487.

Narayanan, V. (2003). Tuberous sclerosis complex: Genetics to pathogenesis. Pediatric Neurology *29*, 404-409.

Neuman, N.A., and Henske, E.P. (2011). Non-canonical functions of the tuberous sclerosis complex-Rheb signalling axis. EMBO Molecular Medicine 3, 189–200.

Neves-Costa, A., Will, W.R., Vetter, A.T., Miller, J.R., and Varga-Weisz, P. (2009). The SNF2-family member FUN30 promotes gene silencing in heterochromatic loci. PLoS One *4*, e8111.

Nijman, S.M.B. (2011). Synthetic lethality: General principles, utility and detection using genetic screens in human cells. Federation of European Biochemical Sciences Letters *585*, 1-6.

Onda, H., Lueck, A., Marks, P.W., Warren, H.B., and Kwiatkowski, D.J. (1999). *Tsc2*$^{+/-}$ mice develop tumors in multiple sites that express gelsolin and are influenced by genetic background. Journal of Clinical Investigation *104*, 687-695.

Perera, S.A., Li, D., Shimamura, T., Raso, M.G., Ji, H., Chen, L., Borgman, C.L., Zaghlul, S., Brandstetters, K.A., Kubo, S., et al. (2009). HER2YVMA drives rapid development of adenosquamous lung tumors in mice that are sensitive to BIBW2992 and rapamycin combination therapy. Proceedings of the National Academy of Sciences of USA *106*, 474–479.

Piedimonte, L.R., Wailes, I.K., and Weiner, H.L. (2006). Tuberous sclerosis complex: molecular pathogenesis and animal models. Neurosurgical Focus *20*, E4.

Poschmann, J., Drouin, S., Jacques, P.-E., El Fadili, K., Newmarch, M., Robert, F., and Ramotar, D. (2011). The peptidyl prolyl isomerase rrd1 regulates the elongation of RNA polymerase II during transcriptional stresses. PLoS One *6*, e23159.

Pourdehnad, M., Truitt, M.L., Siddiqui, I.N., Ducker, G.S., Shokat, K.M., and Ruggero, D. (2013). Myc and mTOR converge on a common node in protein synthesis control that confers synthetic lethality in Myc-driven cancers. Proceedings of the National Academy of Sciences of USA *110*, 11988–11993.

Rallis, C., López-Maury, L., Georgescu, T., Pancaldi, V., and Bähler, J. (2014). Systematic screen for mutants resistant to TORC1 inhibition in fission yeast reveals genes involved in cellular ageing and growth. Biology Open *3*, 161-171.

Roguev, A., Bandyopadhyay, S., Zofall, M., Zhang, K., Fischer, T., Collins, S.R., Qu, H., Shales, M., Park, H.-O., Hayles, J., et al. (2008). Conservation and rewiring of functional modules revealed by an epistasis map in fission yeast. Science *322*, 405-410.

Roguev, A., Wiren, M., Weissman, J.S., and Krogan, N.J. (2007). High-throughput genetic interaction mapping in the fission yeast *Schizosaccharomyces pombe.* Nature Methods *4*, 861-866.

Rosner, M., Freilinger, A., and Hengstschläger, M. (2004). Proteins interacting with the tuberous sclerosis gene products. Amino Acids *27*, 119–128.

Rosner, M., Hanneder, M., Siegel, N., Valli, A., and Hengstschläger, M. (2008). The tuberous sclerosis gene products hamartin and tuberin are multifunctional proteins with a wide spectrum of interacting proteins. Mutation Research *658*, 234-246.

Rosser, T., Panigrahy, A., and McClintock, W. (2006). The diverse clinical manifestations of tuberous sclerosis complex: a review. Seminars in Pediatric Neurology *13*, 27–36.

Roux, P.P., Ballif, B.A., Anjum, R., Gygi, S.P., and Blenis, J. (2004). Tumor-promoting phorbol esters and activated Ras inactivate the tuberous sclerosis tumor suppressor complex via p90 ribosomal S6 kinase. Proceedings of the National Academy of Sciences of USA *101*, 13489–13494.

Ryan, C.J., Roguev, A., Patrick, K., Xu, J., Jahari, H., Tong, Z., Beltrao, P., Shales, M., Qu, H., Collins, S.R., et al. (2012). Hierarchical modularity and the evolution of genetic interactomes across species. Molecular Cell *46*, 691–704.

Sampson, J.R. (2009). Therapeutic targeting of mTOR in tuberous sclerosis. Biochemical Society Transactions *37*, 259–264.

Sen, R., Malik, S., Frankland-Searsby, S., Uprety, B., Lahudkar, S., and Bhaumik, S.R. (2014). Rrd1p, an RNA polymerase II-specific prolyl isomerase and activator of phosphoprotein phosphatase, promotes transcription independently of rapamycin response. Nucleic Acids Research *42*, 9892-9907.

Serfontein, J., Nisbet, R.E.R., Howe, C.J., de Vries, P.J. (2011). Conservation of structural and functional elements of TSC1 and TSC2: A bioinformatic comparison across animal models. Behavior Genetics *41*, 349-356.

Sievers, F., Wilm, A., Dineen, D., Gibson, T.J., Karplus, K., Li, W., Lopez, R., McWilliam, H., Remmert, M., Söding, J., et al. (2011). Fast, scalable generation of high-quality protein multiple sequence alignments using Clustal Omega. Molecular Systems Biology *7*, 539.

Steglich, B., Strålfors, A., Khorosjutina, O., Persson, J., Smialowska, A., Javerzat, J.-P., and Ekwall, K. (2015). The Fun30 chromatin remodeler Fft3 controls nuclear organization and chromatin structure of insulators and subtelomeres in fission yeast. PLoS Genetics *11*, e1005101.

Strålfors, A., Walfridsson, J., Bhuiyan, H., and Ekwall, K. (2011). The FUN30 chromatin remodeler, Fft3, protects centromeric and subtelomeric domains from euchromatin formation. PLoS Genetics *7*, e1001334.

Sun, W., Zhu, Y.J., Wang, Z., Zhong, Q., Gao, F., Lou, J., Gong, W., and Xu, W. (2013). Crystal structure of the yeast TSC1 core domain and implications for tuberous sclerosis pathological mutations. Nature Communications *4*, 1–8.

Taneja, N., Zofall, M., Balachandran, V., Thillainadesan, G., Sugiyama, T., Wheeler, D., Zhou, M., and Grewal, S.I.S. (2017). SNF2 family protein Fft3 suppresses nucleosome turnover to promote epigenetic inheritance and proper replication. Molecular Cell *66*, 50-62.

The European Chromosome 16 Tuberous Sclerosis Consortium. (1993). Identification and characterization of the tuberous sclerosis gene on chromosome 16. Cell *75*, 1305–1315.

Tong, A.H.Y., Lesage, G., Bader, G.D., Ding, H., Xu, H., Xin, X., Young, J., Berriz, G.F., Brost, R.L., Chang, M., et al. (2004). Global mapping of the yeast genetic interaction network. Science *303*, 808-813.

Van Hoof, C., Janssens, V., De Baere, I., de Winde, J.H., Winderickx, J., Dumortier, F., Thevelein, J.M., Merlevede, W., and Goris, J. (2000). The S*accharomyces cerevisiae* homologue YPA1 of the mammalian phosphotyrosyl phosphatase activator of protein phosphatase 2A controls progression through the G1 phase of the yeast cell cycle. Journal of Molecular Biology *302*, 103-120.

Van Hoof, C., Janssens, V., De Baere, I., Stark, M.J.R., de Winde, J.H., Winderickx, J., Thevelein, J.M., Merlevede, W., and Goris, J. (2001). The *Saccharomyces cerevisiae* phosphotyrosyl phosphatase activator proteins are required for a subset of the functions disrupted by protein phosphatase 2A mutations. Experimental Cell Research *264*, 372-387.

van Slegtenhorst, M., Carr, E., Stoyanova, R., Kruger, W.D., and Henske, E.P. (2004). Tsc1$^+$ and tsc2$^+$ regulate arginine uptake and metabolism in *Schizosaccharomyces pombe*. Journal of Biological Chemistry *279*, 12706-12713.

van Slegtenhorst, M., de Hoogt, R., Hermans, C., Nellist, M., Janssen, B., Verhoef, S., Lindhout, D., van den Ouweland, A., Halley, D., Young, J., et al. (1997). Identification of the tuberous sclerosis gene *TSC1* on chromosome 9q34. Science *277*, 805–808.

Wood, V., Gwilliam, R., Rajandream, M.-A., Lyne, M., Lyne, R., Stewart, A., Sgouros, J., Peat, N., Hayles, J., Baker, S., et al. (2002). The genome sequence of *Schizosaccharomyces pombe*. Nature *415*, 871–880.

Wullschleger, S., Loewith, R., and Hall, M.N. (2006). TOR signaling in growth and metabolism. Cell *124*, 471-484.

Xu, K., Liu, P., and Wei, W. (2014). mTOR signaling in tumorigenesis. Biochimica et Biophysica Acta *1846*, 638–654.

Young, J., and Povey, S. (1998). The genetic basis of tuberous sclerosis. Molecular Medicine Today *4*, 313–319.

Zhang, H., Cicchetti, G., Onda, H., Koon, H.B., Asrican, K., Bajraszewski, N., Vazquez, F., Carpenter, C.L., and Kwiatkowski, D.J. (2003). Loss of Tsc1/Tsc2 activates mTOR and disrupts PI3K-Akt signaling through downregulation of PDGFR. The Journal of Clinical Investigation *112*, 1223-1233.

Zheng, Y., and Jiang, Y. (2005). The yeast phosphotyrosyl phosphatase activator is part of the Tap42–phosphatase complexes. Molecular Biology of the Cell *16*, 2119-2127.

Zuk, O., Hechter, E., Sunyaev, S.R., and Lander, E.S. (2012). The mystery of missing heritability: Genetic interactions create phantom heritability. Proceedings of the National Academy of Sciences of USA *109*, 1193-1198.

Ashyad Rayhan

Education

M.Sc. Biology, 2015 – 2017
University of Western Ontario, London, ON, Canada

B.Sc. Honours Biology, June 2014
York University, Toronto, ON, Canada

Work Experience

Graduate Research Assistant, *University of Western Ontario*, 2015 – 2017
Graduate Teaching Assistant, *University of Western Ontario*, 2015 – 2017
Field Research Assistant, *York University*, 2013

Service and Outreach

Seminar Committee, *Society of Biology Graduate Students*, 2015 – 2016
Outreach Committee, *Biology Graduate Research Forum*, 2016

Scholarships and Awards

Biology Graduate Student Travel Award, 2017
Dean's Honour List, B.Sc., 2013
York University Entrance Scholarship, 2006

Peer-reviewed Publications

Rayhan, A., Faller, A., Chevalier, R., Mattice, A., and Karagiannis, J. (2017). Using genetic buffering relationships identified in fission yeast to reveal susceptibilities in cells lacking hamartin or tuberin function. (In Preparation)

Conference Presentations

The 9th International Fission Yeast Meeting, Banff, AB, Canada
Rayhan, A., Faller, A., and Karagiannis, J. (2017). Using genetic buffering relationships identified in fission yeast to elucidate the molecular pathology of tuberous sclerosis. [Talk]

Biology Graduate Research Forum, London, ON, Canada
Rayhan, A., Faller, A., and Karagiannis, J. (2016). Investigation of genetic mutants displaying synthetic sickness with *tsc1* and *tsc2* loss of function mutations in *Schizosaccharomyces pombe*. [Poster]

North East Regional Yeast Meeting, Buffalo, NY, USA
Rayhan, A., Faller, A., and Karagiannis, J. (2016). Investigation of genetic mutants displaying synthetic lethality/sickness with *tsc1* and *tsc2* loss of function mutations in *Schizosaccharomyces pombe*. [Poster]

Joint Meeting of the Entomological Societies of Canada & Ontario, Guelph, ON, Canada
Rayhan, A., Harpur, B., and Zayed, A. (2013). Taxonomically-restricted genes within the honey bee genome. [Poster]